Response to general comments

We thank the Referees for their critical and constructive comments. Both Referees point out that the paper section in which we compare the plume model to high resolution models is partly redundant to previous work and that this section can be shortened. We agree with the Referee 2 that the main focus of the paper should be on its novel results - sensitivity analysis and comparison of plume models to observational data. We modified the manuscript accordingly

In what follows we respond all concerns individually.

Response to all comments
Reviewers' comments are in indented blocks and in *italic*, followed by thy authors response and author's changes in manuscript underlined.

Page and line mentions refer to the marked manuscript unless stated otherwise.

Reviewer 1
Concern #1

> *The first conclusion of the paper states that the plume model reveals a similar qualitative behaviour to the high resolution numerical modelling studies, but this point has already been made by previous studies, e.g. Xu 2012, Slater 2015 and Sciascia et al.*

We agree with this statement, yet this similarity has not been quantified by a scaling number.

We added a literature reference to former work (marked manuscipt, p. 12 line27)

Concern #2

> *The authors list the previous studies on the melt rate dependencies to the external forcing factors, such as ocean temperature and subglacial discharge. This part is written as if the previous results are inconsistent with each other, but it is not.*

We agree with the reviewer that some sentences in this paragraph may make an impression that there are inconsistencies between different results performed with high-resolution 2-d and 3-d models. This was not our intention – instead we wanted to give a short overview of a number of relevant modeling works performed in recent years to study glacier-ocean interaction.

Thus we reformulated this passage to describe the variety of results in the context of diverse environmental conditions and model formulation (p.2 line 22-p.3 line10).

> *For example, it is not fair to compare Sciascia et al. (2013) versus Holland et al. (2008b) and Little et al. (2009). Sciascia et al. (2013) considers the effects of subglacial discharge on the melting of a vertically terminating glacier, while Holland and Little (2008b) considers the effect of circulation inside an ice-shelf cavity on the melting. These papers address different problems.*

Agreed. We now give more details about the glacier type (p.2 line 34 – p.3 line 2).

> *As a result, Sciascia et al. (2013) uses a nonhydrostatic model, whereas the other two studies use hydrostatic models.*

We added this information as a note in the general description about modelling approaches (p.2 line 23), but not in direct relationship with the above-mentioned results, because it is not clear to us why

this particular model formulation should play a role in the resulting melt rate. We assume here, as suggested by the reviewer, that model results are consistent with each other and that differences in melt rate stem from the experimental setting (unless explicitly stated otherwise by the original authors). How much 3D model formulation may influence the results is an interesting question that should be addressed in a different study.

> *The authors states "A closer look on the CP melt rate profiles revealed differences among the 3D models: Kimura et al. (2014) showed a melt rate profile of the CP that reaches its maximum near to the water surface while Slater et al. (2015) and Xu et al. (2013) found a CP melt rate profile with the maximum located near to the bottom." This gives an impression that the numerical models are not consistent with each other.*

> *The authors do not seem to understand that this difference originates from the difference in the model set up. The background stratification in Kimura et al. (2014) is uniform, while Slater et al. (2015) and Xu et al. (2013) employ linearly stratified profiles. The plume reaches its maximum height until it depletes the buoyancy to the surrounding environment, so the plume can reach higher in the uniform environment than the linearly stratified environment for a given amount of discharge (source of buoyancy). There are assumptions that go into setting up these numerical models and depending on the assumptions the outcomes are different.*

We reformulated to make clear that these differences likely come from experimental setting or model parameters (p.3 lines 9-10): "Simulations with 3D models, which differ with respect to boundary conditions and turbulence parameters, show a variety of CP melt rate profiles: ..."

> *As a result, comparing the plume models*
> *and these modelling results by plotting profiles of melt rate, temperature and velocity, such as in Fig 13, 14 and 15, and coming up with a scaling factor do not provide any scientific insights.*

Of course we are aware of the different model setups and in each case we used vertical temperature and salinity profiles **identical** to the corresponding GCM experiment. This was mentioned in LP model section p.10, lines 29-31: "we used the same temperature and salinity profiles as in Sciascia et al. (2-13a) and the same subglacial discharge […]. We used an entrainment factor […] consistent with their experiments.", but was indeed omitted in the CP section. We thus provided additional details about our experimental setting in the CP section p.11 lines 13-15:

"We used the same experimental settings (discharge, salinity and temperature profiles) as in the experiments of the 3D models, with an entrainment rate E0 = 0.1."

However, we do not agree with the reviewer that such comparison does not provide any scientific inside. The aim of our comparison is to test our simple parameterizations against more advanced models. This comparison shows that the simple plume parameterization produced qualitatively rather similar results to much more computationally expensive 3-D model over a large range of melt rates (several orders of magnitude), but to get a quantitative agreement, a constant scaling coefficient in the order of one has to be applied. We also found that the chosen value for the

entrainment coefficient has a significant impact on the simulated melt rate, and thus on the agreement with physically based models. We believe, these are important findings.

We modified point 4) of the conclusions to emphasize this finding:

"We compared the CP and LP models to results of 3D GCM experiments, and find qualitatively similar melt rate profiles. In most cases, the LP model overestimates the results of the GCM by approximately a factor two, while the CP model underestimates melt rate from GCMs. Such discrepancy is not surprising given the highly simplified parameterization of the LP and CP models compared to GCMs. Importantly, we find the same power law dependence of melt rate on subglacial water discharge as in Slater et al. (2016), for given ambient hydrographic conditions. As a result, with a constant scaling factor of the order of one, the simplified models can reproduce a wide range of melt rates spanning several orders of magnitude."

Concern #3

> *Temperature and salinity of the subglacial discharge are set to T0 = 0 and S0 =0, while the model uses the linearlized freezing condition, equation 7. According to the equation 7, the freezing temperature for the freshwater (S0=0) is lambda2 + lambda3*Z. This means that the prescribed subglacial discharge is below freezing at the source (x=0), 0< lambda2 + lambda3*Z, which implies freezing at the source (melt rate below 0). What is the melt rate at the source? Profiles of melt rate presented in the paper, Figure 7, 11 and 12, all seem to indicate above freezing near the source, which seems inconsistent.*

Firstly, contrary to the reviewers' assumption, freezing temperature of freshwater (Ts=lambda2+lambda3*Z) is negative for fjord depths larger than 109m (see Table 2.1 for numerical values), which is the case of all fjords we considered in this study. The later was not stated explicitly and, probably, caused this confusion. We made this point clear in the revised manuscript. As a result, temperature of the plume is always above the freezing point at the source and therefore melt rate is positive (Z< -lambda2/lambda3). As far as the choice of initial temperature T_o=0 ^{o}C is concerned, we believe this is a reasonable assumption. The temperature of subglacial water is unknown, but for obvious reasons it cannot deviate significantly from 0^{o}C. Compared to other uncertainties in plume parameterization, this is probably the least important one. In particular, for conditions typical for the Greenlandic environment, we did not find any significant change in melt rate when using the pressure melting point instead of T_o=0^{o}C, since the plume temperature rapidly converges to a balance temperature close to ambient water temperature (see Appendix Figure A3).

We added a note that Z<0 in the marked manuscript (p.5 line 7).

Concern #4

> *The authors use the entrainment rate of 0.036 to estimate the melt rates of Greenland glaciers. The authors justify this choice by comparing the shape of plume to that from the high-resolution numerical model results of Sciascia 2013 and Xu 2012 (page 10, line 30). I do not understand this justification because Sciascia et al. 2013 calibrates the unresolved process using the entrainment rate of 0.08.*

In fact, we used the same entrainment coefficient as Sciascia et al. 2013 (as indicated p.11 line 13 , p.11 line 27, and displayed in Figure. 13 a). However, we also tested other values for the entrainment coefficient and found that for E0=0.036, plume models are in better agreement with

results from Sciascia et al. 2013 (not shown). We agree that the sentence referred to by the reviewer could be misleading, and we simply removed it along with the reference to our unshown sensitivity tests on E0 (p.11, lines 20-23).

Concern #5

> *The authors conclude that the overestimation of melting by LP is due to the lack of Coriolis term in the plume model. This conclusion comes out of nowhere. There are no constructive arguments to support this point in the paper. The authors need to explain how the Coriolis term changes the plume dynamics and results in lowering the melt rate.*

We thought that this fact is well-known. In particular, this limitation of 1-d plume model has been recognized already in Jenkins (1991) who wrote: “However, in this study the influence of Earth rotation is not considered, so the results are strictly only applicable to regions where the flow is constrained by topography.” and later “This is because the Coriolis force, which is not incorporated in this simple one-dimensional treatment will tend to deflect the flow across the basal slope, hence reducing the sinθ term”.

We added an explanation on the influence of the Coriolis force in the section on Petermann glacier (marked manuscript, p. 12 line 28-31).

We addressed all minor concerns (thanks!): .

Page 1, line 8: computationally instead of “computational”
Done, marked manuscript p.1 line 8.
Page 13, line 14: missing space between “model.” and “Fried”.
Done
Page 13, line 19: the units m and d should be non italic.
Done.
Page 20, line 20: should be “axisymmetric plume” not “axis-symmetric plume”.
Done.
Page 25, line 25: No need to cite the same paper by Sciascia twice.
Done.
Page 14, line 14. missing “.”
Done.
Figure 1, The entrainment should be perpendicular to the rising plume, so the red arrows need to be adjusted

Done, see new manuscipt figure 1a.

Reviewer 2

We thank reviewer 2 very much for the constructive comments and the literature references pointed out. We believe our updated manuscript was much improved in the process.

Reviewers' comments are in indented blocks and in *italic* followed by thy authors response and author's changes in manuscript underlined.

Page and line mentions refer to the marked manuscript unless stated otherwise.

Response to all comments

> *1. Most of the plume scalings presented here recover results derived in previous work, and this is not fully acknowledged in the present manuscript:*

We thank the reviewer for pointing that out. We have now included the missing literature throughout the manuscript, as detailed below.

> *• Section 3 of Slater et al (2016) has previously derived an approximate analytical solution for conical plumes, seemingly with some discrepancies with the present work. It wasn't obvious how these compare to your estimate in equation (13), and in particular how Q depends on z in (13)?*

Our Equation (13) is basically the same as Slater et al (2016) (their Equation (5)) for the initial velocity of a tidewater glacier, except that we account for basal drag Cd.
It describes "balance" velocity **at the grounding line** (it makes use of the relationship between subglacial discharge, initial velocity and initial plume dimension, as a boundary condition, thus with no dependence on z).

We rewrote our section 2.3, including references with Slater et al (2016), to to make that clear, and added the "**sg**" subscript for "subglacial" to **q** (Eq. 12) and **Q** (Eq. 13).

> *Similarly, figure 3 suggests there is convergence to a constant velocity near to the grounding*
> *line, but the analytical and numerical results of Slater et al (2016) suggests the constant value of U breaks down for larger z. Does your scaling hold throughout the depth of the ocean?*

The purpose of Figure 3 (now Figure 2) is to show the initial adjustment of velocity toward the balance velocity over a relatively short distance. The figure shows a large range of initial velocities, over almost two orders of magnitude, which is larger than later evolution in plume velocity with z. What we term "balance velocity" (basically the solution where the U' term is negligible) needs not be constant with z. There is no inconsistency with Slater et al (2016). This is now clearly stated in the rewritten section 2.3. For instance we now write:

"Note that equation (12) is identical to the velocity derived by Jenkins (2011), and equation (13) is analogous to equation (5) in Slater et al. (2016), with the addition of the basal drag term. These balance solutions are only valid in the vicinity of the grounding line and

velocity might then differ substantially as the plume develops, especially for small subglacial discharge (e.g. Magorrian and Wells, 2016)"

> *Finally, the cumulative melt rate for the conical plume is argued here to scale as the 2/5-power of the subglacial discharge, whereas Slater et al (2016) found a 1/3-power dependence (their equation 11). Can you test this discrepancy more carefully?*

This is because this expression only describes the dependence of **initial velocity** on the discharge (the fast initial adjustment was explained for the line plume model in equations A12-14). However the **evolution** of the velocity along the depth of the ocean follows the 1/3 power law that Slater detected.

Note that we now rearranged equation (13) with respect to Qsg to make the **1/5** power law for the initial velocity more apparent.

Also note that contrary to our provisional response in the interactive discussion, we decided not present additional scaling analysis for the cone plume model, because it was already done by Slater et al (2016), and the conical plume geometry does not allow the same reasoning about the volume flux (QU) as was done for the line plume (qU) in the Appendix. We maintain the scaling for the line plume, which is novel.

> • *The scaling inherent in the balance velocity (12) for line plumes with strong subglacial discharge was derived in equation (21) of Jenkins (2011). The corresponding convergence to solutions with an initially uniform velocity (c.f. figure 1.21 and appendix A2) was previously considered in section 3 of Dallaston et al (2015), albeit with a simplified model that captures the leading order behaviour.*
>
> • *The behaviour of the line plume model for small subglacial discharge has been considered in section 3.1 of Magorrian & Wells (2016). The result presented in (A19) recovers this as a limiting case, and it would be good to emphasise these linkages. The current method of asymptotically patching the two limits together (weak and strong subglacial discharge) by considering the total alongslope buoyancy flux is physically elegant and practically useful, so it would be good to emphasise that it recovers the key limits seen in previous work.*

We are grateful to the reviewer for providing these references that corroborate our results for scaling analysis for the line plume. We now acknowledge these authors in our revised section 2.3 and in the appendix, e.g. in the introduction:

"Slater et al. (2016) previously presented approximate analytical solutions for the CP model. Jenkins (2011) noticed that for strong discharge, plume velocity in the LP model does not change much with depth and is thus similar to the initial balance velocity (our equation 12). Magorrian and

Wells (2016) covered the case for small discharge. The reasoning in this appendix provides a unifying solution for small and large discharge with the LP model."

-

> *2. Figure 9b. Your plotted subglacial discharge exponent for line plumes disagrees with the 1/3-power determined by Slater et al (2016), and indeed there is some evidence of a weaker dependence for large discharge in figure 9b. Can this be investigated in more detail?...*
> *A more convincing way to demonstrate a proposed power law scaling* $\dot{m} = aQ_{sg^\beta} + c$ *is via a compensated plot of the form*
>
> $$y = \log\left(\frac{\dot{m} - c}{a}\right)\frac{1}{Q_{sg}} \qquad \text{vs.} \qquad t = \log\left(Q_{sg}\right)$$
>
> *On such a plot, any region of pure power-law scaling produces a constant value equal to the exponent* $y = \beta$

Note that Figure 9b) gave the melt rate dependence for the cone plume (CP), while the line plume (LP) was displayed in 9a). In Fig. 9a), the exponent of the line plumes (1/3) agrees with Slater's work.

Nevertheless our figure 9 b) was inaccurate with respect to power law scaling, and redundant since Slater et al (2016) already addressed the cone plume scaling. Instead we show a log-log plot for the LP in order to illustrate the two limiting regimes of the plume (no dependence for small discharge, cubic root power law for large discharges) (p.29 Figure 6), as suggested by the reviewer.

> *3. Discussion of sensitivity to entrainment rate in section 3.2. The sensitivity of melt rate to entrainment for a line plume can be understood from the previous results of Jenkins (2011) and Magorrian & Wells (2016). The more novel point that you make with figures 6 and 8 is that the uncertainty in E yields quantitative changes to predicted melt rates that are comparable to non-trivial changes in forcing variables such as subglacial discharge and ambient temperature. Some of this section (and the range of figures) could be condensed by exploiting references to earlier studies, and hence highlight your new results more clearly.*

As the reviewer suggested, we will concentrate more on our novel findings in the discussion of the entrainment rate and will shorten this part of discussion with the comparison of earlier studies. We will also eliminate redundant figures.
We referenced to the previous literature (p.9. line 16) and eliminated figure 7 in the old manuscript. To emphasize our new finding we mentioned them in our conclusions part 3 (p.16, line 20-22).

> *Section 3.3. How are the scaling exponents for* $\dot{m} \propto T F\beta$ *determined? These estimates could be compared to the previous scaling results in Slater et al (2016), Jenkins (2011) and Magorrian & Wells (2016) which analytically predict dependences on ambient temperature. Also, simulations with realistic stratifications have been considered previously by Carroll et al (2015), Carroll et al (2016), and the results here should be placed in the context of this previous work.*

The scaling exponents discussed in section 3.3 were determined numerically. .

As suggested by the reviewer we now compare our numerical results with analytical solution presented in the literature, with a new Table 3 referred in the main text.

> *Section 4. The comparison of plume models to general circulation models has been carried out in a range of previous studies (e.g. Sciascia et al 2013, Carroll et al 2015, Kimura et al 2016). (It should also be noted that eddy diffusivities or grid resolution can differ between models and may be tuned to best match the plume model, and thus this might not be a fully independent test of plume theory). I think the paper might read better if this section were cut down to summarise the result wherever a previous comparison is available.*

We shortened this section accordingly to the reviewer suggestion (see previous answers above). We also removed former Figures 13 and 15 that were mostly redundant with findings from Sciascia et al (2013) (but see next reply to comment below) and Slater et al (2015)

> *Also, figure 5 of Sciascia et al (2013) compared a plume model to their numerical results, and obtained a tighter fit than you obtain with the black line in figure 13. Can you explain this discrepancy? Are the same heat and salt transfer coefficients being used?*

According to personal communication with Sciascia, the temperature profiles used in their work was different from ours.

> *6. Section 5. Comparison of plume models to observations. In section 5.2, the observations of Fried et al (2015) were compared to a plume model by Carroll et al (2016), echoing some of your key conclusions. These should be acknowledged appropriately. More generally, the section would benefit significantly from greater synthesis and comparison between the results in different fjords. Can you provide any insight into whether the plume models are capable of predicting melt rates consistent with all the observations within error bars, with a single set of parameters (entrainment, drag, heat and salt transfer coefficients) used throughout?*

We followed the reviewers' constructive suggestion and
added a new subsection (5.5. Summary) and a new Table 6 and figure 16.

> *It would also be worth adding a cautionary note that you sometimes get a misleading picture from estimates of melt rate based on synoptic surveys of ocean heat and freshwater content downstream from the ice. This is due to variability in heat storage in the fjord that might not be captured in a snapshot (Jackson et al*
> *2014).*

We very much agree with adding the cautionary note as it appears to us as a crucial point when comparing model results to observational data. We discuss these limitations of empirical data for testing our modeling approach in the beginning of section 5 (p. 12 line 30-32).

All minor concerns :

> *7. p2 lines 32-35. It would be good to emphasise the different settings considered*

here, which have different force balances (large scale nearly geostrophic flow under a sloping ice shelf vs non-hydrostatic flow next to vertical ice faces).

This has been added (p, 2 line 22,35).

8. Section 2.1.1. Cite the source of the line plume model.

Has been added p.4 line 16

9. Equation (2) omits a term of the form $-\partial/\partial x\, D\, 2\, \Delta\rho g \cos\alpha$ under sloping ice shelves (e.g. see equation 7 of Payne et al 2007, then resolve into components along slope). This might be discussed

We preferred to concentrate solely on the original LP model formulation of Jenkins (2011).

10. Page 6 line 15. Need to define W - presumably the width of the fjord?

Yes, inserted p. 6 line 19.

11. Section 3.4. It may be worth mentioning that the applicability of your plume scalings is confined to warm fjords (if the fjord is close to the freezing temperature, the pressure-dependence of the freezing temperature becomes important as considered by Jenkins, 2011).

We inserted the conditions we used for the scaling analysis in the beginning of the appendix, p.17 line 19.

12. Sections 3.4 and 5.1. Discussion of the Coriolis effect. You should qualify this statement by emphasising that the Coriolis effect is significant for flows with small-to-moderate Rossby number $U/f\, L$. 1, where f is the Coriolis parameter, U the horizontal component of velocity and L the characteristic lengthscale. You might also note the observed channelisation of melt on Petermann noted in Rignot & Steffen (2008), and modelled by Gladish et al 2012 (for example).

We inserted this explanation with reference to the literature in the subsection on Petermann glacier p.13 line 12-14.

13. Section 5.2. Discussion of disagreement for EQUIP. Is it possible that there is a non-trivial rotationally steered outflow here?

We referred to this flow as ’horizontal’ and ‘non-upwelling’ and referenced for further detail on the original paper p.15 line 29.

14. End of section 5.2, discussion of disagreement over undercutting in figure 17. The disagreement might potentially be explained by near surface calving, or local temperature/salinity differences if there is surface run off into the upper ocean very near to the glacier. This could be added to the discussion.

Yes we agree very much to that point and *added a note on that in this section(p.14, line 23-24)*

15. Section 5.4, discussion of Gade and Motyka methods. It would be useful to briefly explain the difference between these cases.

We added a short overview (p.15 line 6-9).

16. Conclusion 3 about the limited effect of entrainment on the melt rate seems to slightly contradict earlier discussion, where you argued the uncertainty corresponds to a 1 ◦ C change in ocean temperature, or significant uncertainty in subglacial discharge.

Agreed, and changed (p.16 line 20-22)

17. Page 15, lines 15-18. Can you clarify what ranges of conditions were considered for this comparison?

Done (p.1*7 line 26-28*).

18. Before equation (A13). Can you clarify in what sense this is an asymptotic solution? I.e. what are you considering to be small or large?

In the sense of a first-order linear differential equation with constant coefficients. It is an analogy because the length scale Lu depends on plume dimension D, which is not constant.
At x=0, Lu is less than a centimeter, whereas our experiments suggest a length scale of one meter for the LP model in some typical conditions. In any case for the LP model, the adjustment occurs over a few meters, and for the CP model a few 10s of meters (Fig. 2a). We agree that asymptotic may be confusing given the physical context. We changed to "equilibrium". We also provide more details and caveats.

19. Combining figures 1 and 2 as (a) and (b) might save some journal pages.

Done, now figure 1.

20. Figure legends. There are inconsistent levels of precision in numerical values in the legends across many figures, and sometimes inconsistencies with the captions. Can the correct values be clarified?
Done for figure 13 and 14.

21. Figure 9 belongs before figures 6-8, according to discussion in the text
Rearranged now figure 5.

22. Figure 10. Would it be more instructive to plot these values per unit width of the fjord, so that they can be compared fairly?

Good point, we adapted this suggestions (Figure 8).

23. Figures 7, 13a,15 illustrate messages from earlier work and might be omitted to cut down on length. Similarly some of figures 1.21-1.23 might be condensed/omitted where the point is clear in earlier work

We agree and omitted figure figure 7, 13a and 15 of the old manuscript and added the literature reference in section 3.2.

24. Figure 1.20. Values of E = 1.6 are unreasonably large. The plume model relies on a boundary layer approximation that the plume is thin compared to its along shelf extent (D << X) which breaks down for large E.

We agree and this was unfortunately just a typo and we corrected it to E=0.16. (*legend*, *Figure 1.16*)

Response to K. Mankoff

> *There is a crisis of reproducibility in science in general, in the earth sciences, and in the cryospheric and oceanic sciences. The Cryosphere is making progress by urging authors to include DOIs for data. I hope the authors, editors, and other reviewers consider the code for this model equivalent to "data", and that a DOI for the code is Included in the final version of this manuscript, if it is accepted for publication.*

We intend to share our model code as soon as the paper is accepted for publication and will upload the script as supplementary material.
A note is added in the new manuscript under Code availability.

Submarine melt parameterization for a Greenland glacial system model

Johanna Beckmann, Mahé Perrette, and Andrey Ganopolski
Potsdam Institute for Climate Impact Research, 14412 Potsdam, Germany
Correspondence to: Johanna Beckmannn (beckmann@pik-potsdam.de)

Abstract. Two hundreds of marine-terminating Greenland outlet glaciers deliver more than half of the annually accumulated ice into the ocean and play an important role in the Greenland ice sheet mass loss observed since the mid 1990s. Submarine melt plays a crucial role in the mass balance and position of the grounding line of these outlet glaciers. As the ocean warms, it is expected that submarine melt will increase and outlet glaciers will retreat, contributing to sea level rise. Projections of the future contribution of outlet glaciers to sea level rise is hampered by the necessity to use extremely high resolution of the order of a few hundred meters both for modelling of the outlet glaciers and as well as coupling them with high resolution 3D ocean models. In addition fjord bathymetry data are mostly missing or are inaccurate (errors of several 100s of meters), which questions the benefit of using ~~computational~~ computationally expensive 3D models for future predictions. Here we propose an alternative approach based on using of computationally efficient parameterization of submarine melt based on turbulent plume theory. We show that such parameterization is in a reasonable agreement with several available modeling studies. We performed a suit of experiments to analyse sensitivity of these parameterizations to model parameters and climate characteristics. We found that the computationally cheap plume model demonstrates qualitatively similar behaviour as 3D ~~gerneral~~ general circulation models. To match results of the 3D models in a quantitative manner, a scaling factor in the order of one is needed for the plume models. We applied this approach to model submarine melt for six representative Greenland glaciers and found that the parameterization of a line plume can produce submarine melt compatible with observational data. Our results show that the line plume model is more appropriate than the cone plume model for simulating the submarine melting of real glaciers in Greenland.

1 Introduction

Since the 1990s the decadal loss of ice mass by the Greenland ice sheet (GrIS) has quadrupled (Straneo and Heimbach, 2013), with an average 1993-2010 contribution of 0.33 ± 8 mm yr^{-1}, which is about 10 % of the observed sea level rise during this period (Church and White, 2011; Church et al., 2013). This acceleration of the GrIS mass loss is attributed to increase of surface melt due to atmospheric warming (Khan et al., 2014) and speedup of the marine-terminating outlet glaciers (Rignot and Kanagaratnam, 2006). The latter has been related, among other factors, to enhanced submarine melting, which in turn is caused by warming of the surrounding ocean (Straneo et al., 2012) and, probably, by increased subglacial water discharge (Straneo and Heimbach, 2013). While ice-ocean interaction potentially plays an important role in recent and future mass balance changes of

the GrIS, the understanding of this interaction remains rather poor and represents one of the main source of the uncertainties in future sea level rise projection (Church et al., 2013).

The ice sheet models used for the study of GrIS response to global warming and its contribution to sea level rise typically have resolution of 5 to 10 kilometers (Bindschadler et al., 2013), which is too coarse to resolve most of Greenland outlet glaciers. Instead, regional modelling at higher resolution is better suited to capture glacier dynamics. As an alternative to costly three-dimensional models, one-dimensional flowline models were convincingly applied to several major outlet glaciers (Nick et al., 2012, 2013; Lea et al., 2014; Carr et al., 2015). In particular, Nick et al. (2012) simulated with a flowline model the dynamical response of the Petermann glacier to the abrupt break up of its floating tongue in 2010 and investigated the influence of increased submarine melting on future stability of the glacier. They demonstrated the strong influence of increased submarine melt rate to the glacier's mass loss. In this study, submarine melt rate was prescribed and held constant. Nick et al. (2013) using the same flowline model implemented submarine melt proportional to the ocean temperature outside of the fjord. This study was performed for the four largest outlet glaciers. Under the assumption that the result of the four largest glaciers can be scaled up for the remaining glaciers, Nick et al. (2013) estimate a total contribution of the Greenland outlet glaciers to global sea level rise of up to 5 cm during the 21st century or about 50% of the maximum expected GrIS contribution due to changes in surface mass balance. For the same period of time but using a three-dimensional ice sheet model, Fürst et al. (2015) estimated the contribution of enhanced ice discharge through outlet glaciers to be 20 to 40% of the total mass loss. These large uncertainties are associated with the parameterization of the rate of submarine melt. Note that in Fürst et al. (2015) the effect of ocean warming was parameterized through enhanced basal sliding rather than explicit treatment of submarine melt.

Different approaches have been derived to calculate submarine melt rates of outlet glaciers by using empirical data (Motyka et al., 2013; Rignot et al., 2015a); simplified one dimensional models of line plumes ~~(Jenkins, 1991; ?), axis-symmetric~~ (Jenkins, 1991, 2011), axisymmetric plume models (Cowton et al., 2015; Turner, 1973) and numerical three-dimensional ~~non-hydrostatic~~ ocean models (3D models) ~~(Xu et al., 2013; Sciascia et al., 2013b; Holland et al., 2008a; Slater et al., 2015)~~(Holland et al., Note that 3D modelling efforts also differ with respect to model formulation, in particular some authors use non-hydrostatic models (e.g. Holland et al., 2008b; Little et al., 2009), while others use hydrostatic models (e.g. Sciascia et al., 2013a). The experiments studied submarine melt with respect to subglacial discharge and its spatial pattern, vertical ocean temperature and salinity profiles. Additionally the influence of the fjord circulation, which connects outlet glaciers with the surrounding ocean, were investigated with the 3D models. Different authors considered two main types of subglacial discharge. The first one is uniformly distributed along the grounding line (referred hereafter as 'line plume', LP) ~~(Jenkins, 1991; ?; Sciascia et al., 2013b; Slater et al., 20~~ the second one is localized (the ~~axis-symmetric~~ axisymmetric plume, referred hereafter as 'cone plume', CP) (Cowton et al., 2015; Turner, 1973; Slater et al., 2015; Xu et al., 2013). The CP approach is motivated by the observations that a significant fraction of subglacial discharge during the melt season emerges through one or several channels underneath the glacier (Rignot et al., 2015b; Stevens et al., 2016; Sole et al., 2011). These simulations, in agreement with previous theoretical studies, show that submarine melt strongly depends both on the ambient water temperature and the magnitude of subglacial discharge. However different modeling studies revealed ~~somewhat different dependences. While Sciascia et al. (2013b)~~ the complex dependence of submarine melting on temperature. Sciascia et al. (2013a) investigated tidewater glaciers and found a linear dependence of the

submarine melt rate on ambient water temperature above freezing point. On the other hand, Holland et al. (2008b) and Little et al. (2009) found a quadratic dependence on temperature under large ice shelves, where geostrophic flow becomes significant. Xu et al. (2013) detected that this relationship of melt rate to thermal forcing depends on the amount of subglacial discharge released through a single channel at a tidewater glacier: the melt rate dependence to temperature has a power of 1.76 for small discharges and is lower for higher discharge. Slater et al. (2016) found a power law dependence of melt rate on discharge, with the exponent ~~$\frac{2}{5}$ for~~ $\frac{1}{3}$ for both the CP and the ~~CP model and $\frac{1}{3}$ for the LP model~~ LP models in a uniform stratification. For a linear stratification their study shows that the exponent enlarges to $\frac{3}{4}$ for the CP model and to $\frac{2}{3}$ for the LP model. A change in power law could also be detected by Xu et al. (2013). They determined an exponent of 0.5 at high and 0.85 at low discharge for the CP. ~~A closer look on the~~ Simulations with 3D models, which differ with respect to boundary conditions and turbulence parameters, show a variety of CP melt rate profiles~~revealed differences among the 3D models~~: Kimura et al. (2014) showed a melt rate profile of the CP that reaches its maximum near ~~to~~ the water surface while Slater et al. (2015) and Xu et al. (2013) found a CP melt rate profile with the maximum located near to the bottom.

While experiments with high-resolution (several to ten meters) nonhydrostatic 3D ocean models demonstrate their potential to simulate rather realistically turbulent plumes and melt rates of marine-based glaciers, such models are too computationally expensive for modeling of the entire Greenland glacial system response to climate change at centennial time scale. An alternative is to use a parameterization of submarine melt based on a simplified plume model ~~(?Cowton et al., 2015)~~(Jenkins, 2011; Cowton et al.,
Such parameterization can then be used to calculate submarime melt in a 1D ice stream models. This would represent a step forward compared to a rather simplistic treatment of submarine melt used in previous works (e.g., Nick et al., 2013).

The main purpose of this paper is to investigate the applicability of the simple plume parameterizations to simulation of melt rate of real glaciers in Greenland. To this end we first compared both cone and linear plume parameterizations with the available results of simulations from high resolution 3D ocean models. Then we compare results of plume parameterizations with the empirical estimates of submarine melt from several Greenland glaciers.

The paper is organized as ~~following~~follows. The two versions of plume model are described in the section 2. There we study the plume models sensitivity of simulated submarine melt rate to ocean temperature and salinity, the amount of subglacial discharge and to the ice tongue geometry of the glacier itself. Results of simulations with the simple plume parameterizations are compared to results of numerical experiments with 3D ocean models in section 4. In section 5 we compare our simulations to empirically estimated submarine melt rates for several selected Greenland glaciers. Finally, in the section 6 we discuss the applicability of the plume parameterization for the purpose of developing a comprehensive Greenland glacial system model.

2 The plume models

A plume model describes buoyancy-driven rise of subglacial meltwater after it exits subglacial channels, until it reaches neutral buoyancy near the surface. Two counteracting processes control its evolution, which are (a) additional melting under the floating tongue (if any) and along the glacier front, and (b) turbulent entrainment and mixing of surrounding fjord water. They act to maintain, or reduce, plume buoyancy, respectively.

Subglacial meltwater discharge Q_{sg} for a glacier can be estimated from surface runoff and basal melt over the catchment area of the glacier. How this discharge is distributed along the grounding line, however, is in general not known. It is believed that at least during summer season, most of the subglacial discharge occurs through a network of channels (Chauche, 2016; Rignot and Steffen, 2008; Rignot et al., 2015b; Schoof, 2010) but their precise number for different glaciers and relative importance is not known and can change throughout the season.

We investigate two situations. The line plume (LP) model corresponds to the simplest assumption that Q_{sg} is uniformly distributed along the grounding line (Fig. 1), while the cone plume (CP) assumes point-wise release of meltwater (Fig. ??1b), i.e. from a channel whose dimensions are small compared to the plume diameter. Note there need not be only one CP: they can be a number of them discretely distributed along the glacier.

2.1 Model equations

Both models are formulated in one dimension, x, which is the distance along the glacier front from the grounding line and depends on the glacier shape, described by its slope α. The model equations are written under the assumption that the plume is in equilibrium and therefore do not explicitly account for time. All model parameters and their description are listed in Table 1.

2.1.1 Line plume

The LP model after Jenkins (2011) accounts for a uniformly distributed subglacial discharge along the grounding line of a glacier (Fig. 1). Far enough from the lateral boundaries, it assumes invariance by translation along the grounding line, so that the resulting equations only depend on x with $\frac{d()}{dx} = ()'$:

$$q' = \dot{e} + \dot{m} \tag{1}$$

$$(qU)' = D\Delta\rho g sin(\alpha) - C_d U^2 \tag{2}$$

$$(qT)' = \dot{e}T_a + \dot{m}T_b - C_d^{\frac{1}{2}} U \Gamma_T (T - T_b) \tag{3}$$

$$(qS)' = \dot{e}S_a + \dot{m}S_b - C_d^{\frac{1}{2}} U \Gamma_S (S - S_b) \tag{4}$$

where the plume state variables D, U, T and S stand for its thickness, velocity in the x-direction, temperature and salinity, all dependent on x. Equation (1) describes the conservation of volume flux $q = DU$ (expressed per unit length in lateral direction, i.e. $\mathrm{m^2 s^{-1}}$), which can increase by the entrainment of ambient seawater $\dot{e}$ and by melting $\dot{m}$ of ice from the glacier front. The momentum flux (Eq. 2), is based on the balance between buoyancy flux and the drag $C_d U^2$ of the glacier front. The buoyancy flux is proportional to the density contrast $\Delta\rho$ between plume water and ambient water in the fjord (subscript a), parameterized in linear form as $\beta_S(S_a - S) - \beta_T(T_a - T)$, with coefficient β_S and β_T indicated in Table 1. The drag also results in a turbulent boundary layer (subscribt b) at the ice-water interface, where melting occurs, and heat and salt is exchanged by (turbulent) conduction-diffusion. The Equations for T and S (Eq. 3,4) account for the entrainment of ambient water and the addition of

meltwater, as well as for conduction fluxes at the ice-water interface (i.e. between boundary layer and plume). The entrainment rate is calculated as $\dot{e} = E_0 U \sin(\alpha)$, proportional to plume velocity and glacier slope, with coefficient E_0. The melt rate is calculated by solving for heat and salt conservation at the ice-water boundary ($\dot{m}$, T_b and S_b are unknown):

$$\dot{m}L + \dot{m}c_i(T_b - Ti - T_i) = cC_d^{\frac{1}{2}} U \Gamma_T (T - T_b) \tag{5}$$

$$\dot{m}(S_b - Si - S_i) = C_d^{\frac{1}{2}} U \Gamma_S (S - S_b) \tag{6}$$

where the subscript i for temperature and salinity refers to the inner ice, and c is the specific heat capacity. The system is closed by an expression of the freezing temperature T_b, which can be linearly approximated as a function of depth Z ($Z < 0$) and salinity of the boundary layer S_b:

$$T_b = \lambda_1 S_b + \lambda_2 + \lambda_3 Z \tag{7}$$

with coefficients λ_i listed in Table 1. For a straight wall, $Z = Z_0 + x \cdot sin(\alpha)$, where Z_0 is the negative depth at the grounding line ($x = 0$). Solving for equations (5-7) yields a second order polynomial equation for the melt rate $\dot{m}$, as a function of plume state variables. Note that ~~?~~ Jenkins (2011) also uses an approximation of the melt rate equations, which resolves in $\dot{m} = M_0 U (T - T_f)$, where $T - T_f$ is the plume temperature above freezing point, and M_0 is a slowly varying function of ice temperature below freezing point. Numerically, M_0 varies from $2.9 \cdot 10^{-6}$ to $0.910^{-9} (^\circ C)^{-1}$ over a $T_i - T_f$ range from $-20^\circ C$ to $0^\circ C$, respectively, and the freezing temperature is roughly $-2^\circ C$ (Annex A). We do not use this approximation in our calculation, but this is nevertheless helpful to interpret some of the results presented in our manuscript, in particular the dependence of the melt rate on plume velocity (Annex A).

2.1.2 Cone plume

The second plume model investigated in this paper is the CP model (Cowton et al., 2015). It differs from the LP model by the geometry of the plume, which resembles the half of an upside-down cone (Fig. ~~??~~ 1b). In that case, the plume has definite dimensions and fluxes are expressed in full units (~~$m^3 s^{-1}$~~ $\mathrm{m^3 s^{-1}}$). A cross-section of the plume is half a disk with area $\frac{\pi}{2} D^2$ where the length scale D is here the cone radius at a given x. The equations (1)-(4) now reform for the CP model by considering melting on the diameter $2D$ and entrainment around the arc πD:

$$Q' = (\pi D)\dot{e} + (2D)\dot{m} \tag{8}$$

$$(QU)' = (\frac{\pi}{2} D^2)\Delta\rho g \sin(\alpha) - (2D) C_d U^2 \tag{9}$$

$$(QT)' = (\pi D)\dot{e} T_a + (2D)\dot{m} T_b - (2D) C_d^{\frac{1}{2}} U \Gamma_T (T - T_b) \tag{10}$$

$$(QS)' = (\pi D)\dot{e} S_a + (2D)\dot{m} S_b - (2D) C_d^{\frac{1}{2}} U \Gamma_S (S - S_b) \tag{11}$$

where variables, parameters and equations have the same meaning as for the LP model, and the volume flux $Q = \frac{\pi D^2}{2} U$ is expressed in cubic meters per second.

2.2 Numerics

For the differential equation system of (1)-(4) and (8)-(11) we choose a classical Runge-Kutta-scheme in which we can regulate the regular grid size Δx. Thus we have control of the numerical calculation time and can easily vary $T_a(Z)$ and $S_a(Z)$ for a stratified environment. Furthermore for glaciers with floating tongues $\sin(\alpha)$ can vary as a function of X and therefore the model can adjust dynamically to the glacier in a coupled glacier-plume version. With these initial conditions for the plume T, S, U, D at $x = 0$ we solve the equations (5)-(7)and firstly determine the melt rate $\dot{m}|_{x_0}$ and the boundary conditions $S_b|_{x_0}$ and $T_b|_{x_0}$. These determined variables serve as the input parameters for the differential euqation system to determine the plume properties at the next step $X_{i+1} = X_i + \Delta x$. This routine is continued to determine the melt rate as a function of x until the plume reaches zero velocity or the water surface.The code is written in Python and Fortran for future coupling.

2.3 Initial conditions and balance velocity

In the rest of the manuscript, for simplicity, we refer to the boundary condition at $x = 0$ as "initial conditions" although the model equations are not time dependent. Since subglacial discharge consists of melt water, the salinity and temperature of subglacial discharge water can be set to zero ($S_0 = 0$ and $T_0 = 0$). For both LP and CP models, initial dimensions (radius or thickness) D_0 and velocity U_0 are not known, but they are tied by subglacial discharge. In the ~~LP case , we have $q_{sg} = \frac{Q_{sg}}{W} = U_0 D_0$~~ CP case $Q_{sg} = \frac{\pi}{2} D_0^2 U_0$ (Fig. 1~~), and in the CP case $Q_{sg} = \frac{\pi}{2} D_0^2 U_0$~~ b) while for the the LP case, the subglacial discharge per glacier width W enters the model equations: $q_{sg} = \frac{Q_{sg}}{W} = U_0 D_0$ (Fig. **??**~~).~~ 1).

It turns out that for a given ~~discharge Q_{sg} the solution is not sensitive to the choice of initial U_0 (Fig. 2 and 3 with $q = q_{sg}$ and $Q = Q_{sg}$, explained below).~~

~~Simulations in a well-mixed environment (ambient water density is constant and does not depend on depth) show that simulated velocity U rapidly converges towards the trajectory of the balance~~subglacial discharge, simulated velocity rapidly adjusts to a "balance" velocity, regardless of the initial velocity ~~U_0~~ (Fig. 2a)~~. This balance velocity at $|x = 0$ can be calculated from equations 1 and 2(Eq. 8and 9for the CP model) by assuming a constant volume and momentum flux with~~ , as already noticed by Dallaston et al. (2015). Analytically, the balance velocity (noted $U_\star(x)$ below) is solution of the plume equations (1)-(2) and (8)-(9) when the transient term U' is neglected. The fast adjustment around $x = 0$ (where plume dimension is small) can be explained by some rearranging into a form analogous to a first order ~~approximation of $\dot{m} << \dot{e}$ (see A, Eq. A15):~~

$$U_{\star 0} = \left(\frac{q g \Delta\rho|_{x_0} \sin(\alpha)}{E_0 \sin(\alpha) + C_d} \right)^{\frac{1}{3}}$$

~~for~~ linear differential equation for U^2 (see Appendix section A2.2). The balance velocity is not necessarily constant, but a simple expression for $U_{\star 0}$ (at $x = 0$) can be derived, if the plume dimension is expressed as a function of subglacial discharge, and the ~~LP model and with the same assumptions:~~

melt rate is neglected compared to entrainment in the volume flux equations (1) and (8) (see Appendix section A1). We obtain for the LP:

$$U_{\star 0} = \left(\frac{Qg\Delta\rho|_{x_0}\sin(\alpha)}{\sqrt{Q2\pi(E_0\sin(\alpha)+2\frac{C_d}{\pi})}} \frac{g\Delta\rho|_{x_0}\sin(\alpha)}{E_0\sin(\alpha)+C_d} q_{sg} \right)^{\frac{2}{5}\frac{1}{3}} \tag{12}$$

and for the CP~~model with ($Q = \frac{\pi}{2} D^2 U$) . The corresponding profiles of melt rate (Fig. 2 b)~~ :

$$U_{\star 0} = \left(\frac{\pi}{2} \frac{(g\Delta\rho|_{x_0}\sin(\alpha))^2}{(\pi E_0\sin(\alpha)+2C_d)^2} Q_{sg} \right)^{\frac{1}{5}} \tag{13}$$

Note that equation (12) is identical to the velocity derived by Jenkins (2011), and equation (13) is analogous to equation (5) in Slater et al. (2016), with the addition of the basal drag term. These balance solutions are only valid in the vicinity of the grounding line and velocity might then differ substantially as the plume develops, especially for small subglacial discharge (e.g. Magorrian and Wells, 2016). More detailed discussion and full, depth-dependent solution for the LP model are given in the Appendix.

Our sensitivity tests show that initial velocities higher than $U_{\star 0}$ lead to maximum melting near the bottom of the glacier ('undercutting') while for lower velocities the ~~maximum is reached a bit higher~~ melt rate increases with height and would leave a so-called 'toe' at the glacier bottom ~~.~~

~~Due to the convergence of U_0 to U_b, cumulative melt rate is not sensitive to the initial velocity, except for very high (unrealistic) values of initial velocity~~ (Fig. ~~3). In both plume models~~ 2b). We checked that initial velocities smaller than the balance velocity yield very small difference in the cumulative melt rate (Fig. 3), although some differences occur for larger velocities. For the LP model an initial velocity ten times larger than the balance velocity gives a 10% higher melt rate while the CP model produces 25% more melting (Fig. 3).

Since the velocities of subglacial discharge are mostly unknown, these results prompted us to use ~~this balance velocity as an~~ the balance velocity of Eqs. (12) and (13) as initial condition in all experiments described below~~if not~~ , unless stated otherwise.

2.4 Default experimental setting

In the next sections we perform a number of sensitivity studies with respect to key parameters. To that end we choose a default experimental setting as a benchmark. Unless otherwise stated, we consider a 500-m deep, well-mixed fjord with ambient temperature $T_a = 4°C$ and salinity $S_a = 34.65\,\mathrm{psu}$ (maximal melting conditions for Greenlands fjord), with total subglacial water discharge of $\mathrm{q_{sg}} = 0.1\,\mathrm{m^2 s^{-1}}$ for the LP model or $\mathrm{Q_{sg}} = 500\,\mathrm{m^3 s^{-1}}$ for the CP model (which ~~is the maximal discharge of Store glacier along a~~ corresponds approximately to the discharge in August 2010 of the 5 km wide ~~glacier front in order to~~ Store glacier (Xu et al., 2012)). Since we apply our model to Greenland fjords, most of them do not have a floating tongue

(tidewater glaciers) ~~, we~~ and we therrfore generally perform experiments for a vertical wall ($sin(\alpha) = 1$). Default model parameters, including entrainment rate E_0, are indicated in Table 1.

A direct comparison between LP (defined per unit length) and CP (point-wise) models, requires an assumption about a length scale W (for LP) and the number of sources (for CP) over which subglacial discharge is distributed. For the CP model we assumed that the entire subglacial discharge occurs through one channel in the center of the glacier (Q_{sg}). In the case of the LP model we assumed that the discharge is uniformly distributed over a fjord width $W = 150m$, so that $q_{sg} = 3.6m^2/s$. This width is about the maximum size of the plume in the CP model, near the surface.

2.5 Comparison between LP and CP models

Results in Figure 4 show that simulated, local melt rate is higher in the CP model than in the LP model practically for all depths, but cumulative melt rate (i.e. integral of the meltrate from the bottom and across entire surface area of the glacier front, of width W) is much higher for the LP model because of the larger surface area over which melting occurs (roughly a factor two in our chosen setting).

We shall see later in this manuscript (sec. 3.1) that the (local) melt rate in the LP model varies less than linearly with subglacial discharge parameter q_{sg}, and thus for a given total discharge Q_{sg}, cumulative LP-induced melt increases with width. As a result, for a wide glacier (i.e. the glacier which is much wider than the maximum diameter of the CP), the LP model gives much higher cumulative melt rate compared to the CP model, when assuming the existence of a single subglacial channel. The situation when there are more than one channel is discussed in section 4.3.

3 Sensitivity experiments

3.1 Subglacial discharge

It is known that melt rate depends strongly on subglacial discharge. In agreement with previous studies ~~(?Cowton et al., 2015)~~ (Jenkins, 201 model shows a cubic root-dependence of the cumulative melt rate on discharge for the LP (~~Fig.5a) and the power of 2/5~~ for the high discharge range) and for the CP ~~(Fig. 5b)~~ in a well-mixed environment~~for the high discharge range~~. Note that for the LP this dependence can already be determined by the look on the balance velocities $U_{\star 0}$ (Eq. 12 ~~and 13~~). However for smaller discharge in a well-mixed environment, cumulative melt rate converges to a small but not insignificant value that does not ~~obe~~ obey the power law any more (Fig. 5~~a) and b)~~. This value represents background melt rate which does not depend on discharge and can be representative for winter melt rate when subglacial discharge is very small. To explain this change of power law we ~~undetook~~ undertook a dimensional analysis to obtain theoretical solutions for the plume model (A). Important is that, in a well mixed fjord, the melt rate is linear dependent on the velocity of the plume. This velocity is dependent on discharge and rather constant over the glacier front for big discharge or independent on sublgacial discharge and will accelerate along the x direction for small discharges (Annex A3, Fig. A2). Therefore one can ~~sepaerate~~ separate the plume behaviour into regimes for

high and low discharges. We also derived an analytical solution for the cumulative melt rate (Eg. A20) that is also displayed in Figure 5.

However, as mentioned in the introduction, stratification can change this power law. We also performed experiments with stratification as in (Xu et al., 2013) for different discharges with the CP model and LP model. The CP model shows values close to Xu et al. (2013). Both models show an increasing exponent for lower discharge (Tab. 2).

3.2 Entrainment rate

Entrainment is the mechanism through which the volume flux of the plume increases with distance from its source, as warmer, saltier fjord water mixes into the plume. This leads to more heat available for melting, but on the other hand to decreased buoyancy - and velocity - as the plume gets saltier. Slower velocity as a result negatively affects melting (Eq. 5, 6) (Carroll et al., 2016) (note the plume also becomes thicker to accomodate for increased volume flux and decreased velocity). In this section we investigate what is the net effect of these processes on melting for typical plume configurations.

In both plume models, entrainment depends on an entrainment rate parameter E_0 (sec. 2.1), which is not accurately known and can be regarded as a tunable parameter within a certain range of values known from pevious work. Laboratory experiments for a pure vertical plume and model studies gives for E_0 a broad range from 0.036 to ~~1.6 (?McConnochie and Kerr, 2016; Kaye and Linden,~~ (Jenkins, 2011; McConnochie and Kerr, 2016; Kaye and Linden, 2004; Mugford and Dowdeswell, 2011; Carroll et al., 2015b; Kimura et

~~In our simulations with the LP model~~ It is known that the cumulative melt for tidewater glaciers ~~(Fig. 6), we obtain a decrease in cumulative melt rate~~ decreases with increasing E_0 (Jenkins, 2011; Magorrian and Wells, 2016) (in the reported range of E_0 values~~. In that case, the melting is therefore~~). The melting is controlled in first order by the plume velocity and only to a lesser extent by availability of heat through mixing ~~. A closer look at vertical profiles of melting, velocity, temperature confirms this interpretation (Fig. ??). Figure shows that~~ for stong subglacial discharge (Magorrian and Wells, 2016). Moreover the relative effect of entrainment can dominate the effect of the ambient temperature (Fig. (7)). E.g. A LP with low entrainment E_0 in a colder ambient temperature of $T_a = 3°\mathrm{C}$ will result in higher cumulative melt rate (due to its higher velocity) than for a plume with high E_0 in a warmer fjord of $T_a = 4°\mathrm{C}$.

For the CP model (Fig. 6c) the dependence on E_0 is opposite: cumulative melt rate increases with the entrainment factor. This is due to the faster growing plume radius with higher entrainment, which leads to a larger area of the plume in contact with the ice, and thus to more melting overall, despite the lower local melt rate.

3.3 Ambient temperature and stratification

Different fjords are characterized by different temperature and salinity profiles. Since the temperature of the ocean is projected to increase with global warming, dependence of melt rate on ocean temperature is crucial to study glaciers response to global warming. Previous experiments with 3D ocean models showed different behavior of the cumulative melt rate as a function of the ambient temperature T_a. Figure 8 shows for both plume models the dependence of cumulative melt rate on temperature in a well-mixed ambient environment for different values of subglacial discharge. Both models show for small discharge a

non-linear dependence of the melt rate on water temperature. If the discharge is very small, ambient properties dominate the melting process and one can speak of a 'melt driven convection' (Slater et al., 2015).

If we assume a power law dependence of the cumulative melt rate per glacier area to the thermal forcing, i.e. ~~$\dot{m} \propto TF^{\beta}$, where $TF = T_A - T_f$ and T_f~~ $\bar{m} \propto TF^{\beta}$, where $TF = T_a - T_{af}$ and T_{af} is the freezing temperature of the sea water at the fjord bottom, we find that the exponent β increases with lower discharge. From 1.2 (high discharge $q = 0.1\ m^2 s^{-1}$) to ~~1.6~~ 1.8 $q = 10^{-6} m^2 s^{-1}$ for the LP , and from 1.2 (high discharge ~~300 $\mathrm{m^3 s^{-1}}$) to 1.4~~ 500 $\mathrm{m^3 s^{-1}}$) to 1.5 (low discharge ~~$Q_{sg} = 0.030\ \mathrm{m^3 s^{-1}}$~~ $Q_{sg} = 0.005\ \mathrm{m^3 s^{-1}}$) for the CP. For the LP the range of this increment compares well to analytical solutions while the CP model seems not to show this change in power law for analytical solutions (table 3).

~~This is also the case~~ An increment of the power law has also been detected when we use a realistic stratification (Fig. 9b). For the LP, we calculated an exponent of 1.2 for high discharge and 1.4 for low discharge, while the CP model shows a similar increase from 1.1 to 1.3. Carroll et al. (2015a) showed that plume thoery gives a good approximation of the outflow height for 3d nonhydrostatic plume model but nevertheless do the exponents differ slightly in the experiment by Xu et al. (2013) (table 3).

3.4 Glacier front angle

The Glacier front angle $\sin(\alpha)$ linearly impacts buoyancy (Eq. 2) and entrainment. For glaciers with a floating tongue, and therefore a smaller angle ($\sin(\alpha) << 1$), entrainment is reduced and so the temperature of the plume (10 c).The dependence of melt to the slope of the glacier has been derived by Magorrian and Wells (2016) but note that the choice of E_0 can have a similar effect as the choice of subglacial discharge as depicted in Figure 10.

A glacier with a long floating tongue, and therefore a smaller angle (i.e. $\sin(\alpha) = 0.02$), has a smaller average melt rate than a tidewater glacier. However in this case higher E_0 leads to higher cumulative melting (Fig.6 b). These high cumulative melt rates (Fig.10) occur due to the longer distance under a floating tongue in which the velocity accelerates (10 b). The theroetical ~~explention~~ explanation of the evolution of U, $\dot{m}$, T is explained in the Annex (A and summarized in A3). However, for small α both plume models are not applicable along the total shelf because they do not take into account Coriolis force and therefore likely strongly overestimate plume velocity and melt rate (see more in section 5.1).

4 Comparison with general circulation models

4.1 Background

Studies of turbulent plumes caused by subglacial discharge and their effect on submarine glacier melting have been performed using 2D and 3D non hydrostatic general circulation ocean models (GCM) (Sciascia et al., 2013a; Xu et al., 2012, 2013; Kimura et al., 2014; Slater et al., 2015). Although these models contain the right physics to simulate plume dynamics, the problem is that it requires very high spatial resolution which is computationally too expensive for our purpose. In order not to resolve the small-scale turbulences, a parameterization for turbulent diffusivity is chosen to represent subgrid-scale mixing. Kimura

et al. (2014) and Slater et al. (2015) tuned the diffusivity in such a way that the ~~axis-symmetric~~ axisymmetric simulated plume (without ice contact) showed the same characteristics as the analytical models of Turner (1973) and Morton et al. (1956). Xu et al. (2013) used a high spatial resolution in order to resolve turbulence explicitly. These models were run for idealized fjord configuration with constant subglacial discharge and a vertical ice front. In most LP experiments, where subglacial discharge was uniformly distributed along the glacier grounding line, 2D settings were chosen. The melt rate in these experiments was computed using equations (5 -7). Since these models are more advanced compared to simple plume parameterization used in this study, it is informative to compare results of plume parameterization with these models.

4.2 Line plume simulations

~~Figure 11a shows a comparison of~~ We compare the melt rate profiles obtained in the experiments by Sciascia et al. (2013a) with the LP model. Sciascia et al. (2013a) used a 2D GCM with a single 10 m wide grid cell for the width and a 600m deep and 160 km long with a resolution of 10 m $\times$ 10 m. For this simulation we used the same temperature and salinity profiles as in Sciascia et al. (2013a) and the same subglacial discharge per unit of glacier front ($q_{sg} = 0.43\,\mathrm{m^2 s^{-1}}$). We used an entrainment factor of E_0 =0.08 consistent with their experiments. ~~As seen in the figure, the~~ The vertical melt rate profile of the simulated LP model ~~resembles~~ resembled that of the melt rate simulated by the 2D GCM model but is systematically overestimated by the LP model. If we apply a scaling factor of 0.48 to the results of the LP model, the two profiles are in ~~resonable~~ reasonable agreement. Still, there are some differences. The melt rate simulated by Sciascia et al. (2013a) declines with height while the LP model simulates a constant melt rate over a broad depth interval. This is due to the fact ~~,~~that the plume model is not applicable in the vicinity of the fjord surface. A similar effect is seen in the 2D experiment of Xu et al. (2012) in figure 11 ~~b~~a). Again, the LP model overestimates the melt rate but when scaled up by a factor of 0.75, it yields reasonable agreement with the GCM results of Xu et al. (2012). ~~In both cases an entrainment factor of $E_0 = 0.08$ was chosen for the LP model. This value is close to the middle of the literature range. Using the value $E_0 = 0.036$ (which is probably unrealistically small) the LP model simulates a shape of the melt rate profile more close to GCMs but even stronger overestimates the melt rate such that a scaling factor of 0.4 for Sciascia et al. (2013a) and of 0.7 for Xu et al. (2012) is needed (not shown).~~

4.3 Cone plume simulations

For the channelized subglacial discharge the most recent, numerical experiments (and most in agreement with plume theory) by Slater et al. (2015) and Xu et al. (2013) were compared with simulations of the CP model. We used the same experimental settings (discharge, salinity and temperature profiles) as in the experiments of the 3D models, with an entrainment rate $E_0 = 0.1$. Xu et al. (2013) used results of a survey to Store Glacier (500m deep and 5km wide) performed in 2010, in particular the observed temperature and salinity profile. They performed simulations of plumes for different discharge values but same diffusivity for a 150 m wide, 500 m deep fjord with a 1m resolution near the glacier. Their sensitivity study showed that uncertainty in channel width yielded 15% uncertainty in the cumulative melt rate. Fig. ~~??~~ 11 b) shows the dependence of the cumulative melt rate on the discharge for a single plume from Xu et al. (2013) and the CP model. Both models reveal a similar

dependence of melt rate on discharge, but the CP model underestimates the melt rate compared to the 3D GCM. To bring the two melt rates in better agreement a scaling factor of 3.4 needed for the CP model~~is needed~~.

Slater et al. (2015) used a coarser resolution GCM with parameterized turbulence. They calibrated the GCM (vertical plume, without ice) against pure plume theory for each applied discharge value by adjusting the diffusivity until plume properties (temperature, salinity, thickness and velocity) matched plume theory by Turner with $E_0 = 0.1$ (personal communication from D. Slater). Turners plume theory is similar to our CP model (eq. 8-11) but omits the terms with melt rate $\dot{m}$ and drag C_d. After tuning, the GCM was applied to simulate the melt rate for the same discharge values and diffusivity for a vertical ice front.Furthermore a minimum velocity of $U_0 = 0.04ms^{-1}$ was intoroduced to create a backround melting the is calclutated with Equation (5-7)

~~Figure ?? shows the cumulated melt rate simulated in Slater et al. (2015) for the total subglacial discharge of $500\,\mathrm{m^3 s^{-1}}$ equally distributed through n=1, 2, 3, 5, 10, 50 channels and evenly distributed over the whole glacier width.Similar experiments performed with only the CP model, show that the CP model consistently underestimates cumulative melt rate compared to the GCM. The agreement can only be achieved by multiplying the CP model results by a factor 2.5. If we use the CP model and calculate the background melt rate equal to the experiment, we still need a factor of~~ .In order to simulate the the same cumulative malt rate as Slater et al. (2015) distributed by $1-10$ channels a scaling factor is needed of 2.46 without a backround melting and 1.7 ~~to match our results to Slater et al. (2015). However, in the case of a large number of channels, the CP model, which cumulative melt rate simply follows $\dot{m} \propto n(\frac{Q}{n})^{\frac{2}{5}}$, significantly overestimates the melt rate simulated with the GCM. The CP model handles each plume seperately and unlike the GCM, can not simulate the interaction between many cones, which might coalesce and act more like our LP model~~with background melting is needed. On the other hand, the result of the GCM for the same total subglacial discharge but uniformly distributed along the whole grounding line is rather close to the results of the LP model. Indeed, for this case Slater et al. (2015) received the cumulative melt rate of $3.69\,\mathrm{md^{-1}}$, while for the LP model we receive $2.42\,\mathrm{md^{-1}}$ for $E_0 = 0.1$ and $3.71\,\mathrm{md^{-1}}$ for $E_0 = 0.036$.

4.4 Conclusions

From these comparison of simple parameterizations with physically-based model it appears that the LP model needs to be scaled down (except for Slater et al. (2015)) and the CP model scaled up. The scaling factor is in the order of one. Most importantly CP and LP models reveal a similar qualitative behavior to much more complex and computationally demanding GCMs as shown in Xu et al. (2012); Slater et al. (2015); Sciascia et al. (2013a).

5 Comparision with empirical data

Few studies exist where submarine melt has been calculated directly based on field measurements. We used here the available data to test the LP and CP models against observations. However the results have to be observed with caution since a single temperature profile does not necessarily represent the average heat storage in a fjord since it can undergoe great variability (Jackson et al., 2014).

5.1 Petermann glacier

For the the years 2002-2006 Rignot and Steffen (2008) calculated the melt rate of the floating tongue of Petermann glacier obtained from velocity measurements and mass balance. They detected 4 big channels of along the floating tongue. Due to its long floating tongue, the estimated melt rate is reliable because it is less affected by errors in estimating the calving rate as it is the case for tidewater glaciers. For modeling the melt rate of Petermann glacier we used temperature and salinity profile in the fjord in front of the floating tongue measured in the year 2003 by Johnson et al. (2011b). We also use the data from Morlighem et al. (2014) to define the margins of the Petermann glacier and to compute average one-dimensional profile of the floating tongue. We then use a polynomial fit to smooth the profile of the floating tongue. Fig. 12 a) shows the annual mean melt rate calculated with the LP model for $E_0 = 0.08$ and $E_0 = 0.036$. Even for a minimum discharge of $10^{-4}\,\mathrm{m^2 s^{-1}}$ (as discussed in section 3.1) and with $E_0 = 0.036$, the LP model significantly overestimates the melt rate beyond a very narrow range (few km) directly next to the grounding line. This is an expected result, because for long floating tongues at a certain length L Coriolis force becomes important ~~which~~ for small to moderate Rossby numbers R and a (horizontal) plume velocity U if $\frac{U}{fL} < 1$. At this length scale the plume flow gets deflected (to the right here) and will be domintad by geostrophic flow as modelled by Gladish et al. (2012). Yet this is not taken into account in our simple plume model, as discussed in section 3.4. On the other hand, when using the CP model and a large discharge given by the total runoff over the catchment area distributed over four identical subglacial channels, we receive very low melt rates (Fig. 12b). It is clear that the LP model is in better agreement than the CP model at simulating the melt rate near the grounding line of the Petermann glaciers but correction for Coriolis effect is required further from the grounding line.

5.2 West Greenland glaciers

In a small fjord in West Greenland the melt rate of four glaciers was determined by measuring salinity, temperature and velocity in the fjord near the glacier fronts (Rignot et al., 2010). In Torrsukatak fjord (TOR) the average and cumulative melt represents the melt rates of both glacier fronts together (Seermeq Avangnardleq and Sermeq Kujatdleq) since the fronts are situated in the same head of the fjord branch. The two other glaciers, Kangilerngata Sermia (KANGIL) and Equip Sermia (EQUIP) enter different fjords. Measured velocity in front of EQUIP does not show an upwelling pattern but more a right to left circulation, nevertheless we also calculated the melt rate with our plume models for EQUIP. For all glaciers we took the total width of the glacier to determine the subglacial discharge per unit of length for the LP model and determined the average depth of the grounding line as a starting point for the LP model. We then compare our simulations to the average melt rate determined by Rignot et al. (2010). As shown in the experiment by Slater et al. (2015), a large number of channels acts like a LP but we also computed cumulative melt assuming the existence of one big single CP starting at the maximum depth of the grounding line. Table 4 shows the ratio between observed and simulated melt rate for two types of plume models and two values of entrainment rate factor E_0. For KANGIL and EQUIP results of the LP model are in reasonable agreement with measurements, especially for the smallest E_0 value (45%-105%). Although for EQUIP the agreement is the best with the LP model, the lack of upwelling

circulation indicates that the plume parameterization may not be applicable to this glacier and therefore this agreement may be a pure coincidence. The melt rate ratio of one CP shows rather poor results (1%-5%).

We also compared our model with the data from Fried et al. (2015) for ~~Kanderlussuq~~ Kangerlussuup Sermia glacier which is located in West Greenland northward of previously discussed glaciers. We used data from Morlighem et al. (2014) for the glacier elevation and after averaging to a one dimensional profile we obtained a shelf of 3 km length. Note that caution is needed since the data set is averaged over 10 years and has a resolution of 300m. Realistic temperature stratification can lead to maximal melting at the bottom of tidewater glaciers near the grounding line (e.g. Fig. 9a). This maximal melting at the bottom may cause so-called undercutting, which may enhance mass loss by calving (Rignot et al., 2015a). Fried et al. (2015) found that 80% of the tidewater glacier is undercut by 45 meters in average. The glacier releases subglacial discharge via two big channels, but their corresponding melting contributes only 15% of the total melt of the glacier front. Furthermore Carroll et al. (2016) showed that the simulated melt rate of a single cone plume is about 2 magnitudes lower than the spatially averged melt rate by Fried et al. (2015). Thus we investigate whether the LP model can calculate the average melting by assuming that the 250 meter deep glacier is undercut below 50 meters depth, with an angle of 77° to achieve the observed undercutting (Fig. 13a). Bartholomaus et al. (2016) give the belonging CTD data and estimate an summer discharge. We use the CTD closet to the glacier front in Summer ~~2014~~ 2013 and the mean summer discharge (~~$208 m^3 s^{-1}$~~ $208\,\mathrm{m^3 s^{-1}}$) per glacier width (3km) as input data for the LP model. Fried et al. (2015) find a total melt rate of 2 md^{-1} for the whole calving front. They assumed that the glacier is only undercut by submarine melting, such that the distance of grounding line to the overhang position subtracted by the glacier's velocity gives the submarine melt value. With this input data and an entrainment rate factor of $E_0 = 0.036$ we achieve an average melt rate of ~~1.7~~ 1.5 md^{-1} (Fig.13). This value is close to the empirical data but this plume would not result in the mentioned undercutting depth, since it ~~penetraites up to 1m~~ penetrates up to 10 meter below the sea surface. The entrainment factor $E_0 = 0.16 - 0.13$ lets the plume stop at 50 m depth but their melting corresponds only to 50% of the empirical data for the total melt rate. If the the LP model is correct it means, that additional fjord circulation make out 50% of the melting.Furthermore deriving the melt rate by one CTD profile close to the glacier might be diluted by near local surface runoff or calving an thus cooling and freshening of the surface ocean waters.

5.3 Helheim

Sutherland and Straneo (2012) used results of a field campaign in Semerlik fjord in summer 2009 where temperatures, salinities and velocities were measured at seven stations in the fjord to calculate the melt rate of Helheim glacier. We applied the temperature and salinity ~~profiles of their section 3~~ profile closest to the glacier (section 7) for the LP model to simulate the melt rate ~~in order to compare it~~for comparison. We assume, following Sutherland and Straneo (2012), that Helheim glacier is a tidewater glacier and has a depth of 700 m and a width of 6 km and the subglacial discharge of ~~5.1 $\mathrm{km^3 a^{-1}}$ (summer in 2007-2008; Andersen et al., 2010)~~ $5.1 \pm 0.76\,\mathrm{km^3 a^{-1}}$ (summer in 2008; Andersen et al., 2010). Figure 14 shows ~~our best fit to the values. We computed~~ the simulated melt rates over for different E_0 with the average subglacial discharge. Our best fit computes an average melt rate of ~~1.7 md^{-1} (Sutherland 1.7 md^{-1}~~ 1.6 md^{-1} (Sutherland 1.8 md^{-1}) with an entrainment factor ~~$E_0 = 0.04$~~ $E_0 = 0.036$.

5.4 Store Glacier

Another well documented glacier is Store glacier. Xu et al. (2013) estimated an average submarine melt rate of ~~4.5 ± 1.5~~ 3.0 ± 1.0 md^{-1} in summer (sec. 4) while new calculations, due to new bathymetry data reveal a melt rate of 4.5 ± 1.5 md^{-1} (Chauche, 2016). Additionally, Chauche (2016) conducted a survey to determine average melt rate and subglacial discharge from November 2012 until May 2013. Two different techniques were used, which we reference as Gade (Gade, 1979) and Motyka (Motyka et al., 2003) in Figure 15 a). The Motyka technique is based on conservation of heat, salt and volume. The Gade-technique is based on the identification and quantification of different processes (i.e. submarine melting, runoff-mixing, thermal cooling, local sea ice formation) that modify the water coloumn by it's tempreature and salinity in certain - for the process - typical gradients. We used the LP model with $E_0 = 0.036$ and an input subglacial discharge determined by Motyka and Gade with the corresponding temperature and salinity profiles, to simulate melt rates. Results from the LP model are biased low compared to the measurements (Figure 15 b), with melt rate underestimated by 75% in average (Table 5). Note that the Motyka method comes with large error bars for both subglacial discharge and corresponding melt rate, which accomodate for the LP model bias (Figure 15). Stated uncertainties for the Gade method are smaller and are not consistent with the LP model results.

5.5 Summary

We tested both line and cone plume models against available empirical data for melt rate, and the line plume was best suited to reproduce observations (Table 4). Table 6 and Figure 16 provide for each glacier the measured discharge and melt rate, with error bars, and corresponding range in simulated melt rate (when errors in observed discharge are taken into account as input). When default drag, heat and salt transfer coefficients are used, the simulated melt rate tends to underestimate observed melt rate, thus the best match was obtained with an entrainment rate $E_0 = 0.036$, on the lower end of our range (e.g. see Fig. 7 for how melt rate varies with E_0). Nevertheless, three glaciers (Helheim, Equip Sermia and Kangerlussuup Sermia) out of seven match observations within the error bars. Varying other model parameters can change the mean but not the spread of simulated melt rate across glaciers and discharge ranges. For instance, if the heat exchange coefficient is increased to $\Gamma_T = 4.2 \cdot 10^{-2}$ (instead of the default $\Gamma_T = 2.2 \cdot 10^{-2}$), the bias can be reduced and simulated melt rates are close with obervations (Helheim and Equip Sermia fall out, conversely). Figure 16 shows a comparison of measured and simulated melt rate with the modified heat transfer coefficient Clearly, many fjord processes are not taken into account in this simplified approach. For example, the circulation in front of Equip Sermia was mostly horizontal (Rignot et al., 2010), instead of the vertical upwelling represented in the model. There are also issues with the measurements themselves, such as time sampling or difficulties to retrieve discharge and melt rate, as seen for the Store glacier (Fig. 15), or for Helheim, where CTD profiles for temperature and salinity were taken one year after discharge rates measurements. Nevertheless, the simple line plume model is in general agreement with the observations (Fig. 16) - and shows a correlation coefficient of 0.7 (Fig. 16 b) with the modified heat transfer coefficient. The theoretical background and similar dependency on discharge compared to more complex models (see previous sections) make

it suitable for modelling studies over a larger number of Greenland glaciers, and to investigate melt rate response to future changes in discharge and temperature. .

6 Conclusions

1) We presented two parameterizations for simulation of the submarine melt rate of marine-terminated glaciers, the so-called cone plume and line plume models and studied sensitivity of these two models to different forcings (fjord temperature, stratification, subglacial discharge) and model parameter (entrainment parameter E_0). We also compared these models with results of experiments performed with 2D and 3D ocean GCM by Slater et al. (2016) and Xu et al. (2013). At last we compared the results of simulations of the LP and CP models with empirical estimates of melt rate for several Greenland glaciers.

2) We found that for small subglacial discharge, typical for winter conditions, cumulative melt does not depend on the discharge. For high discharge typical for summer conditions we found a power dependence of 1/3 of submarine melt on subglacial discharge for the LP models, and a power of 2/5 for the CP model, which is consistent with the previous studies. We found a theoretical explenation of this behaviour, explained in the Annex A. Furthermore we found that the power dependence to the ambient temperature in a well-mixed environment also is 1.7-1.8 for lower discharges and is only 1.2 for the higher discharge for both models.

3) We investigated the sensitivity of the melt rate to the entrainment parameter E_0 that was used parametrization of the turbulence of the plume. For a tidewater glacier the cumulative melt rate of the LP model increases with decreasing E_0 while it decreases for the CP model. This is explained by the fact that although in both cases higher entrainment rate slows down the plume and reduces the melt rate per unit of area, for the CP, this effect is overcompensated by the widening of plume for the higher entrainment coefficient. In general, we found a ~~rather limited effect of entrainment parameter of~~ notable effect of the entrainment parameter on the melt rate for the range of entrainment parameter given in the literature. The uncertainty range of E_0 can have the same effect as 1°C change in ocean temperature.

4) ~~When we compare~~ We compared the CP and LP ~~model~~ models to results of 3D GCM experiments, ~~we find the same dependence of the melt rates on subglacial water discharge but a scaling factor in the order of one was always needed to match our results with the GCMs~~and find qualitatively similar melt rate profiles. In most cases~~(except in Slater et al. (2016))~~, the LP model overestimates the results of the GCM by approximately a factor two, while the CP model underestimates melt rate ~~compare to all GCM results. This is true even for the experiment of Slater et al. (2016), who tuned their GCM to a certain entrainment rate factor E_0 using plume theory~~from GCMs. Such discrepancy is not surprising given the highly simplified parameterization of the LP and CP models compared to GCMs. Importantly, we find the same power law dependence of melt rate on subglacial water discharge as in Slater et al. (2016), for given ambient hydrographic conditions. As a result, with a constant scaling factor of the order of one, the simplified models can reproduce a wide range of melt rates spanning several orders of magnitude.

5) In the case of the long floating tongue, like the Petermann glacier, the LP model significantly overestimates the melt rate outside of the narrow zone along the grounding line which is probably due to the missing Coriolis force in the plume models.

6) Although it is known that in summer a part of the subglacial meltwater is delivered in the fjord through several channels, we found that the submarine melt rate associated with the discharge through the channels and better described by the CP model, makes out only a small amount of the empirically estimated total melt rate of a glacier front. Furthermore the total number of channels for every summer is unknown for different glaciers. When we compare the LP model to empirical data, it is evident that the LP model is more appropriate than the CP model for simulation of both winter and summer melt of real Greenland glaciers. However, the model has to be adjusted for individual glaciers since the scaling parameter is not the same for different glaciers. Thus, for the futue we will use the tuned LP model coupled to a 1d ice flow model to determine the importance of submarine melt rate to glacier dynamics.

Code availability. The Code for the line and cone plume, written in Python, is avaible as supplementary material.

Appendix A: Semi-analytical solutions for the LP model

In this appendix, we analyze the LP model equations in order to derive approximate analytical solutions. This in turn helps to interprete the results of the numerical experiments presented in this paper, performed with the more complete plume models from ?Jenkins (2011). Slater et al. (2016) previously presented approximate analytical solutions for the CP model. Jenkins (2011) noticed that for strong discharge, plume velocity in the LP model does not change much with depth and is thus similar to the initial balance velocity (our equation 12). Magorrian and Wells (2016) covered the case for small discharge. The reasoning in this appendix provides a unifying solution for small and large discharge with the LP model.

We restrict the analysis to the typical conditions of a 500m deep greenladic fjord (T_a $(0-4°C)$).

A1 Simplified melt rate equation

After ?Jenkins (2011), the melt rate can be approximated as

$$\dot{m} \approx M_0 \cdot U \cdot \Delta T \tag{A1}$$

where $\Delta T = T - T_f$ is the temperature above freezing and M_0 is a slowly varying ice temperature below freezing point, which can be considered constant for the purpose of this appendix. Freezing point temperature is given by $T_f = \lambda_1 S + \lambda_2 + \lambda_3 Z$.

We run several experiments in a typical parameter range for tidewater and long floating tongue glaciers in Greenland's fjords and could confirm that the approximation is accurate for the LP model (Fig. A1a). The Parameters varied were Ta $(0-4°C)$,g_{sg} $(1 \cdot 10^{-5} - 0.1)$, E_0 (0.036-0.16) and $\sin\alpha$ (0.02-1) for constant depth of 500m, $T_i = -15°C$ and $S_a = 34.2$. With linear regression we found an average value for ~~$M_0 = 8.2 \cdot 10^{-6}$ for $T_i = -15°C$~~ $M_0 = 8.8 \cdot 10^{-6}$.

Let $T_e = \frac{E_0}{M_0} \sin\alpha$, the entrainment-equivalent temperature ($°C$), be a measure of the ratio of entrainment to melting (it corresponds to the temperature for which melting equates entrainment). We have:

$$\frac{\dot{m}}{\dot{e}} \approx \frac{\Delta T}{T_e} \ll 1 \tag{A2}$$

in all these experiments (Fig. A1b), consistently with the ranges for E_0 (0.036-0.16) and $\sin\alpha$ (0.02-1), so that T_e spans two orders of magnitude, roughly $10^2 - 10^4\ ^\circ C$.

A2 Balance regime

In Figure 2 we showed that CP velocity rapidly converges regardless of initial velocity. ~~Figure ?? shows that for tidewater glaciers with large subglacial discharge, the LP velocity, temperature, salinity~~ This has been also shown by Dallaston et al. (2015) for the LP and also holds for the plume temperature, salininty and melt rate~~converge rapidly as well~~. Here we derive analytical solutions for these convergence values (indicated with $_\star$) and associated length scales for the our approximation of the LP model (i.e. (A1) and (A2)), by using the equation for the volume flux (1) so that:

$$(qX)' = q'X + qX' = (\dot{e} + \dot{m})X + qX' \tag{A3}$$

where $q = DU$ (the volume flux) and X can be any of the T, S or U. The convergence value $X_\star$ can be obtained by solving the corresponding equation $(qX)' = f$ (where f is the right-hand side term, e.g. (2), (3) or (4)) with $X' = 0$. Moreover, when the right-hand side term is not or weakly dependent on X (i.e. for T and S, as will be detailed below), the equation is analogous to a first order differential linear equation with convergence length scale $L_X = \frac{q}{q'} \approx \frac{q}{\dot{e}} = \frac{D}{E_0 \sin\alpha}$, i.e. with fast convergence near the grounding line, where plume thickness D is small.

A2.1 Balance temperature and salinity

Temperature and salinity equations (3) and (4) can be rewritten as an intuitive mixing law by merging in (5) and (6):

$$(qT)' = \dot{e}T_a + \dot{m}T_m \tag{A4}$$

$$(qS)' = \dot{e}S_a \tag{A5}$$

where T_m is an effective meltwater temperature, derived from (5):

$$T_m = c_i/cT_i - L/c + T_b(1 - c_i/c) \approx c_i/cT_i - L/c \tag{A6}$$

Variations of boundary layer temperature T_b around $0^\circ C$ can be safely neglected compared to latent heat, so that we will treat T_m as a constant. If $T_i = -15^\circ C$, we have $T_m \approx -92^\circ C$. Nevertheless for completeness, note that T_b can be expressed as a function of melt rate, plume and ice temperatures from equation (5). Using our simplified melt rate equation (A1) and given that $\dot{m} \ll C_d^{\frac{1}{2}} \Gamma_T U$ by two orders of magnitude, an accurate approximation for T_b is given by:

$$T_b - T_f = \left(1 - \frac{c_i M_0 (L/c_i - T_i)}{c C_d^{\frac{1}{2}} \Gamma_T}\right) \Delta T \approx 0.3 \Delta T \tag{A7}$$

where we verify that boundary layer temperature is somewhat closer to freezing temperature than to plume temperature. In the case of plume salinity S_b cancels out completely and $S_i = 0$ (as can be verified straightforwardly using (4) and (6)), so no other term is needed.

Equations (A4) and (A5) can also be combined with (1) to obtain an expression for plume buoyancy flux:

By decomposing (A4) as outlined in (A3), and searching for solutions when $T' = 0$, with $\dot{m} \ll \dot{e}$, we obtain an expression for balance temperature:

$$T_\star \approx T_a + \frac{\dot{m}}{\dot{e}}(T_m - T_a) \tag{A8}$$

which can be rearranged by using (A2), and neglecting the second order T_a/T_e, into:

$$\Delta T_\star \approx \frac{\Delta T_a}{1 - T_m/T_e} \tag{A9}$$

so that

$$\left(\frac{\dot{m}}{\dot{e}}\right)_\star \approx \frac{\Delta T_a}{T_e - T_m} \tag{A10}$$

The ratio $-T_m/T_e$ spans about 10^{-2} to 1 in our experiments. Here the the freezing temperature implied by Δ should be taken for balance plume salinity, which is nearly the same as ambient salinity in first approximation (Eq. (A5), (A2), (A10)):

$$S_\star = \frac{\dot{e}}{\dot{e} + \dot{m}} S_a \approx (1 - \frac{\dot{m}}{\dot{e}}) S_a \approx (1 - \frac{\Delta T_a}{T_e - T_m}) S_a \approx S_a \tag{A11}$$

so that $\Delta T_\star \approx T_\star - T_{fa}$ and $\Delta T_a \approx T_a - T_{fa}$, where T_{fa} is the freezing temperature for ambient salinity.

A2.2 Balance velocity

A similar reasoning as in the previous section (using (A3) and $q' \approx \dot{e}$), (1) and (2) can be rearranged into an equation for U^2 (note the identity $(U^2)' = 2UU'$):

$$\frac{1}{2}(U^2)' + \frac{(C_d + C_e)}{D} U^2 = b \tag{A12}$$

where $b = \sin(\alpha) g \Delta\rho$ and $C_e = E_0 \sin\alpha$. This highlights in one equation basic plume dynamics, buoyancy-accelerated and balanced by drag and entrainment.

Equation (A12) is analogous to a first order linear differential equation with ~~asymptotic solution~~ equilibrium solution for $x >> L_u$

$$U_\star = \sqrt{\frac{b \cdot D}{C_d + C_e}} \tag{A13}$$

and length scale

$$L_u = \frac{D}{2(C_d + C_e)} \tag{A14}$$

Note that equation (A13) does not represent a strict equilibrium but a dynamic balance between velocity, plume thickness and buoyancy, which is maintained while the plume ~~'s~~ thickness and associated volume flux keeps increasing. ~~This approximation~~

~~is valid in the initial development phase of the plume when the thickness D is small and the volume flux is mostly controlled by velocity. We verify our experimental result~~ Note that as the plume dimension increases with entrainment, so does the length scale L_u, and the feedback balance becomes looser. At $x = 0$ for typical discharge and entrainment values L_y is less than a centimeter. Our simulations show that velocity reaches dynamic balance $U_\star$ within the first few meters after the grounding line (not shown). This shows qualitative agreement with the above analysis but which suggests that initial changes in plume dimension D and buoyancy b should be taken into account for more detailed analysis of the transient regime. In the present analysis we focus on the balance regime. The theoretical equilibration length scale for velocity is shorter than for temperature and salinity by a factor 2 or more, since $L_{TS}/L_U = 2(1+\frac{C_d}{E_0 sin\alpha})$, especially for long floating tongues. In the actual simulations the ratio is even larger, because the plume keeps growing with distance from its source.

Equation (A13) can also be expressed as a function of plume's volume flux q:

$$U_\star = \left(\frac{q \cdot b}{C_d + C_e}\right)^{\frac{1}{3}} \tag{A15}$$

with $q = q_{sg}$ and $b = b_0$ at $x = 0$. In the case of fjord without stratification ($T'_a = 0$ and $S'_a = 0$), we have an expression for the buoyancy flux qb from (A4) and (A5):

$$(qb)' = \dot{m} b_m \tag{A16}$$

where $b_m = g \sin\alpha(\beta_S S_a - \beta_T(T_a - T_m))$ is the meltwater buoyancy minus the heat sink required to melt the ice. Note the temperature account for about 15% of buoyancy variations. According to (A1) the melt rate is proportional to U, thus in the regime where $U \approx U_\star$, we obtain a new differential equation for $U'_\star$. By elevating (A15) at the third power and differentiating, we can use (A16) and the identity $(U^2)' = 2UU'$ to obtain:

$$(U_\star^2)' = \frac{2}{3}\frac{b_m}{C_d + C_e} M_0 \Delta T \tag{A17}$$

By integration,

$$U_\star^2 = U_{\star 0}^2 + \int_0^x (U_\star^2)' dx \approx U_{\star 0}^2 + (U_\star^2)' x \tag{A18}$$

where $U_{\star 0}$ is the balance velocity at $x = 0$, given by (A15), and $\Delta T \approx \Delta T_\star$ in $(U_\star^2)'$ and finally by replacing $\Delta T_\star$ with (A9), we obtain:

$$U_\star(x) \approx \sqrt{\left(\frac{q_{sg} \cdot b_0}{C_d + C_e}\right)^{\frac{2}{3}} + \frac{2}{3}\frac{b_m}{C_d + C_e}\frac{M_0 \Delta T_a}{1 - T_m/T_e} x} \tag{A19}$$

where $b_0 = g \sin\alpha(\beta_S S_a - \beta_T T_a)$ is the buoyancy at x=0 (equal to meltwater buoyancy). See Table A1 for a summary of the variables defined in the appendix.

A2.3 Cumulative melt rate

By integrating equations (A1) with (A9) and (A19), we obtain an expression for the cumulative melt rate in the LP model:

$$M(x) = \int_0^x \dot{m} dx \approx M_0 \Delta T_\star \int_0^x U_\star(x) dx = \frac{C_d + C_e}{b_m} \left(U_\star^3(x) - U_{\star 0}^3 \right) \tag{A20}$$

The error of (A20) compared to the cumulative melt rate of the LP model in the unstratified case for tidewater glaciers was 2 % for big discharge ($q = 0.1 m^2 s^{-1}$) and 9 % for small discharge($q = 1 \cdot 10{-}6 m^2 s^{-1}$). For the case of a long floating tongue and a discharge of $q = 0.1 m^2 s^{-1}$ the error was in the range of 10 %.

A3 The role of subglacial discharge and the shape of the glacier

We investigated the plume properties and melt rate of a typical tidewater glacier and a glacier with a long floating tongue (order of ~~Peterman~~ Petermann glaicer). While for the tidewater glacier the plume temperature rapidly approaches the temperature of the ambient water (Fig. A3 c) the plume under a long floating tongue stays cooler since the melt-entrainment ratio becomes bigger (A8). A look on the velocity of the plume shows an acceleration under floating tongues. Equation (A19) reveals that for a tidewater glacier, a plume starting wit a velocity $U_{\star 0}$, which is dependent on the subglacial discharge, will accelerate with a slope independent of the subglacial discharge. Therefore plumes with small discharges will highly accelerate while the velocity of plumes with big discharge will remain almost constant along Z (Fig. A2) as reported by Dallaston et al. (2015). That explains the different exponents of melt rate as a function of subglacial discharge in the literature. In the case of a very small discharge $q_{sg} \to 0$ then ~~$U_{\star 0} \to 0$~~ $U_\star \to \sqrt{\frac{2}{3} \frac{b_m}{C_d + C_e} \frac{M_0 \Delta T_a}{1 - T_m/T_e} x}$ and the melting becomes independent of the discharge and we speak of the background melting. Magorrian and Wells (2016) undertook a scaling analysis for the plume model for small discharges. For $q_{sg} \to 0$ comparision shows that in our analysis velocity accelerates with $U(x) \sim \sqrt{\sin(\alpha) X}$ equal to the results of Magorrian and Wells (2016). The cumulative melt rate for small discharges in dependence to the thermal forcing ΔT_a gives a power law of 3/2, also confirmed by the work of Magorrian and Wells (2016). For tidewater glaciers with very high discharge the acceleration term (A17) can be neglected and therefore the velocity - and thus the melt rate- depends on the initial conditions of subglacial discharge with the cubic root. Also the melt rate is then linear dependent on ΔT_a. Our approximation of $U_\star$, $T_\star$ and $m_\star = M_0 \cdot \Delta T_\star \cdot U_\star$ are displayed along the LP models results in Figure A3 and show good agreements. The approximation of the cumulative melt rate (A20) shows the biggest deviation for the floating tongue with 10 %.

Author contributions. J. Beckmann and A. Ganopolski designed the study and conducted the analysis. J. Beckmann implemented the numerical models and performed the experiments. M. Perrette and J. Beckmann derived the analytical solutions. J. Beckmann prepared the manuscript with contribution from all authors.

Acknowledgements. This work was funded by Leibniz-Gemeinschaft: WGL Pakt für Forschung SAW-2014-PIK-1. We thank David Sutherland for the CTD - data of ~~Kanderlussuq Sermia~~Kangerlussuup Sermia,Fiamma Stranero and Dustin Carroll fpr the CTD - data of Helheim and Donald Slater for providing us with the data of his experiment. Further more we thank Adrian Jenkins of providing us with his plume code to compare our simulated melt rate profiles among the models. Thanks to Reinhard Calov for support in numerical procedures.

References

Andersen, M. L., Larsen, T. B., Nettles, M., Elosegui, P., Van As, D., Hamilton, G. S., Stearns, L. A., Davis, J. L., Ahlstrm, A. P., De Juan, J., Ekstrm, G., Stenseng, L., Khan, S. A., Forsberg, R., and Dahl-Jensen, D.: Spatial and temporal melt variability at Helheim Glacier, East Greenland, and its effect on ice dynamics, Journal of Geophysical Research: Earth Surface, 115, 1–18, doi:10.1029/2010JF001760, 2010.

Bartholomaus, T. C., Stearns, L. A., Sutherland, D. A., Shroyer, E. L., Nash, J. D., Walker, R. T., Catania, G., Felikson, D., Carroll, D., Fried, M. J., Noël, B. P. Y., and Van Den Broeke, M. R.: Contrasts in the response of adjacent fjords and glaciers to ice-sheet surface melt in West Greenland, Annals of Glaciology, pp. 1–14, doi:10.1017/aog.2016.19, http://www.journals.cambridge.org/abstract{_}S0260305516000197, 2016.

Bindschadler, R. A., Nowicki, S., Abe-OUCHI, A., Aschwanden, A., Choi, H., Fastook, J., Granzow, G., Greve, R., Gutowski, G., Herzfeld, U., Jackson, C., Johnson, J., Khroulev, C., Levermann, A., Lipscomb, W. H., Martin, M. A., Morlighem, M., Parizek, B. R., Pollard, D., Price, S. F., Ren, D., Saito, F., Sato, T., Seddik, H., Seroussi, H., Takahashi, K., Walker, R., and Wang, W. L.: Ice-sheet model sensitivities to environmental forcing and their use in projecting future sea level (the SeaRISE project), Journal of Glaciology, 59, 195–224, doi:10.3189/2013JoG12J125, 2013.

Carr, J. R., Vieli, A., Stokes, C. R., Jamieson, S. S. R., Palmer, S. J., Christoffersen, P., Dowdeswell, J. A., Nick, F. M., Blankenship, D. D., and Young, D. A.: Basal topographic controls on rapid retreat of Humboldt Glacier, northern Greenland, Journal of Glaciology, 61, 137–150, doi:10.3189/2015JoG14J128, 2015.

Carroll, D., Sutherland, D. a., Shroyer, E. L., Nash, J. D., Catania, G. a., and Stearns, L. a.: Modeling Turbulent Subglacial Meltwater Plumes: Implications for Fjord-Scale Buoyancy-Driven Circulation, Journal of Physical Oceanography, p. In press, doi:10.1175/JPO-D-15-0033.1, http://journals.ametsoc.org/doi/abs/10.1175/JPO-D-15-0033.1, 2015a.

Carroll, D., Sutherland, D. a., Shroyer, E. L., Nash, J. D., Catania, G. a., and Stearns, L. a.: Modeling Turbulent Subglacial Meltwater Plumes: Implications for Fjord-Scale Buoyancy-Driven Circulation, Journal of Physical Oceanography, p. In press, doi:10.1175/JPO-D-15-0033.1, http://journals.ametsoc.org/doi/abs/10.1175/JPO-D-15-0033.1, 2015b.

Carroll, D., Sutherland, D. A., Hudson, B., Moon, T., Catania, G. A., Shroyer, E. L., Nash, J. D., Bartholomaus, T. C., Felikson, D., Stearns, L. A., Noël, B. P. Y., and van den Broeke, M. R.: The impact of glacier geometry on meltwater plume structure and submarine melt in Greenland fjords, Geophysical Research Letters, pp. 1–10, doi:10.1002/2016GL070170, http://doi.wiley.com/10.1002/2016GL070170, 2016.

Chauche, N.: Glacier-Ocean interaction at Store Glacier (West Greenland), 2016.

Church, J., Clark, P., Cazenave, A., Gregory, J., Jevrejeva, S., Levermann, A., Merrifield, M., Milne, G., Nerem, R., Nunn, P., Payne, A., Pfeffer, W., Unnikrishnan, D. S., and A.S.: Sea level change, Climate Change 2013: The Physical Science Basis. Contribution of Working Group I to the Fifth Assessment Report of the Intergovernmental Panel on Climate Change, pp. 1137–1216, doi:10.1017/CB09781107415315.026, 2013.

Church, J. A. and White, N. J.: Sea-Level Rise from the Late 19th to the Early 21st Century, Surveys in Geophysics, 32, 585–602, doi:10.1007/s10712-011-9119-1, 2011.

Cowton, T., Slater, D., Sole, A., Goldberg, D., and Nienow, P.: Modeling the impact of glacial runoff on fjord circulation and submarine melt rate using a new subgrid-scale parameterization for glacial plumes, Journal of Geophysical Research: Oceans, pp. n/a–n/a, doi:10.1002/2014JC010324, http://doi.wiley.com/10.1002/2014JC010324, 2015.

Dallaston, M. C., Hewitt, I. J., and Wells, A. J.: Channelization of plumes beneath ice shelves, Journal of Fluid Mechanics, pp. 109–134, doi:10.1017/jfm.2015.609, 2015.

Fried, M. J., Catania, G. A., Bartholomaus, T. C., Duncan, D., Davis, M., Stearns, L. A., Nash, J., Shroyer, E., and Sutherland, D.: Distributed subglacial discharge drives significant submarine melt at a Greenland tidewater glacier, Geophysical Research Letters, 42, 9328–9336, doi:10.1002/2015GL065806, 2015.

Fürst, J. J., Goelzer, H., and Huybrechts, P.: Ice-dynamic projections of the Greenland ice sheet in response to atmospheric and oceanic warming, The Cryosphere, 9, 1039–1062, doi:10.5194/tcd-8-3851-2014, http://www.the-cryosphere-discuss.net/8/3851/2014/, 2015.

Gade, H. G.: Melting of ice in Sea Water: A primitive Model with Application to the Antartic Iceshelf and Icebergs, American Metrological Society, pp. 189–198, 1979.

Gladish, C. V., Holland, D. M., Holland, P. R., and Price, S. F.: Ice-shelf basal channels in a coupled ice/ocean model, Journal of Glaciology, 58, 1227–1244, doi:10.3189/2012JoG12J003, 2012.

Holland, D. M., Thomas, R. H., de Young, B., Ribergaard, M. H., and Lyberth, B.: Acceleration of Jakobshavn Isbr{æ} triggered by warm subsurface ocean waters, Nature Geoscience, 1, 659–664, doi:10.1038/ngeo316, 2008a.

Holland, P. R., Jenkins, A., and Holland, D. M.: The Response of Ice Shelf Basal Melting to Variations in Ocean Temperature, Journal of Climate, 21, 2558–2572, doi:10.1175/2007JCLI1909.1, http://journals.ametsoc.org/doi/abs/10.1175/2007JCLI1909.1, 2008b.

Jackson, R. H., Straneo, F., and Sutherland, D. A.: Externally forced fluctuations in ocean temperature at Greenland glaciers in non-summer months, Nature Geoscience, 7, 503–508, doi:10.1038/ngeo2186, http://www.nature.com/ngeo/journal/v7/n7/full/ngeo2186.html?WT.ec{_}id=NGEO-201407, 2014.

Jenkins, A.: A one-dimensional model of ice shelf-ocean interaction, 96, 671–677, 1991.

Jenkins, A.: Convection-Driven Melting near the Grounding Lines of Ice Shelves and Tidewater Glaciers, Journal of Physical Oceanography, 41, 2279–2294, doi:10.1175/JPO-D-11-03.1, http://journals.ametsoc.org/doi/abs/10.1175/JPO-D-11-03.1, 2011.

Johnson, H. L., Münchow, a., Falkner, K. K., and Melling, H.: Ocean circulation and properties in Petermann Fjord, Greenland, Journal of Geophysical Research, 116, C01 003, doi:10.1029/2010JC006519, http://doi.wiley.com/10.1029/2010JC006519, 2011a.

Johnson, H. L., Münchow, A., Falkner, K. K., and Melling, H.: Ocean circulation and properties in Petermann Fjord, Greenland, Journal of Geophysical Research, 116, C01 003, doi:10.1029/2010JC006519, http://doi.wiley.com/10.1029/2010JC006519, 2011b.

Kaye, N. B. and Linden, P. F.: Coalescing axisymmetric turbulent plumes, Journal of Fluid Mechanics, 502, 41–63, doi:10.1017/S0022112003007250, 2004.

Khan, S. a., Kjaer, K. H., Bevis, M., Bamber, J. L., Wahr, J., Kjeldsen, K. K., Bjork, A. a., Korsgaard, N. J., Stearns, L. a., van den Broeke, M. R., Liu, L., Larsen, N. K., and Muresan, I. S.: Sustained mass loss of the northeast Greenland ice sheet triggered by regional warming, Nature Clim. Change, 4, 292–299, doi:10.1038/nclimate2161, http://dx.doi.org/10.1038/nclimate2161{%}5Cn10.1038/nclimate2161{%}5Cnhttp://www.nature.com/nclimate/journal/v4/n4/abs/nclimate2161.html{#}supplementary-information, 2014.

Kimura, S., Holland, P. R., Jenkins, A., and Piggott, M.: The Effect of Meltwater Plumes on the Melting of a Vertical Glacier Face, Journal of Physical Oceanography, 44, 3099–3117, doi:10.1175/JPO-D-13-0219.1, http://journals.ametsoc.org/doi/abs/10.1175/JPO-D-13-0219.1, 2014.

Lea, J. M., Mair, D. W. F., Nick, F. M., Rea, B. R., van As, D., Morlighem, M., Nienow, P. W., and Weidick, a.: Fluctuations of a Greenlandic tidewater glacier driven by changes in atmospheric forcing: observations and modelling of Kangiata Nunaata Sermia, 1859–present, The Cryosphere Discussions, 8, 2005–2041, doi:10.5194/tcd-8-2005-2014, http://www.the-cryosphere-discuss.net/8/2005/2014/tcd-8-2005-2014.html, 2014.

Little, C. M., Gnanadesikan, A., and Oppenheimer, M.: How ice shelf morphology controls basal melting, Journal of Geophysical Research, 114, C12 007, doi:10.1029/2008JC005197, http://doi.wiley.com/10.1029/2008JC005197, 2009.

Magorrian, S. J. and Wells, A. J.: Turbulent plumes from a glacier terminus melting in a stratified ocean, Journal of Geophysical Research: Oceans, 121, 4670–4696, doi:10.1002/2015JC011160, 2016.

McConnochie, C. D. and Kerr, R. C.: The turbulent wall plume from a vertically distributed source of buoyancy, Journal of Fluid Mechanics, 787, 237–253, doi:10.1017/jfm.2015.691, http://www.journals.cambridge.org/abstract{_}S0022112015006916, 2016.

Morlighem, M., Rignot, E., Mouginot, J., Seroussi, H., and Larour, E.: Deeply incised submarine glacial valleys beneath the Greenland ice sheet, Nature Geoscience, 7, 418–422, doi:10.1038/ngeo2167, http://www.nature.com/doifinder/10.1038/ngeo2167, 2014.

Morton, B. R., Taylor, G., and Turner, J. S.: Turbulent Gravitational Convection from Maintained and Instantaneous Sources, Proceedings of the Royal Society A: Mathematical, Physical and Engineering Sciences, 234, 1–23, doi:10.1098/rspa.1956.0011, 1956.

Motyka, R. J., Hunter, L., Echelmeyer, K. A., and Connor, C.: Submarine melting at the terminus of a temperate tidewater glacier, LeConte Glacier, Alaska, U.S.A, Annals of Glaciology, 36, 57–65, doi:10.3189/172756403781816374, 2003.

Motyka, R. J., Dryer, W. P., Amundson, J., Truffer, M., and Fahnestock, M.: Rapid submarine melting driven by subglacial discharge, LeConte Glacier, Alaska, Geophysical Research Letters, 40, 5153–5158, doi:10.1002/grl.51011, http://doi.wiley.com/10.1002/grl.51011, 2013.

Mugford, R. I. and Dowdeswell, J. A.: Modeling glacial meltwater plume dynamics and sedimentation in high-latitude fjords, Journal of Geophysical Research: Earth Surface, 116, 1–20, doi:10.1029/2010JF001735, 2011.

Nick, F. M., Luckman, a., Vieli, a., Van Der Veen, C. J., Van As, D., Van De Wal, R. S. W., Pattyn, F., Hubbard, a. L., and Floricioiu, D.: The response of Petermann Glacier, Greenland, to large calving events, and its future stability in the context of atmospheric and oceanic warming, Journal of Glaciology, 58, 229–239, doi:10.3189/2012JoG11J242, 2012.

Nick, F. M., Vieli, A., Andersen, M. L., Joughin, I., Payne, A., Edwards, T. L., Pattyn, F., and van de Wal, R. S. W.: Future sea-level rise from Greenland's main outlet glaciers in a warming climate, Nature, 497, 235–238, doi:10.1038/nature12068, http://www.nature.com/doifinder/10.1038/nature12068, 2013.

Rignot, E. and Kanagaratnam, P.: 'Changes in the Velocity Structure of the Greenland Ice Sheet', Science, 311, 986–990, doi:10.1126/science.1121381, 2006.

Rignot, E. and Steffen, K.: Channelized bottom melting and stability of floating ice shelves, Geophysical Research Letters, 35, doi:10.1029/2007GL031765, 2008.

Rignot, E., Koppes, M., and Velicogna, I.: Rapid submarine melting of the calving faces of West Greenland glaciers, Nature Geoscience, 3, 187–191, doi:10.1038/ngeo765, http://dx.doi.org/10.1038/ngeo765, 2010.

Rignot, E., Fenty, I., Xu, Y., Cai, C., and Kemp, C.: Undercutting of marine-terminating glaciers in West Greenland, Geophysical Research Letters, 42, 5909–5917, doi:10.1002/2015GL064236, 2015a.

Rignot, E., Fenty, I., Xu, Y., Cai, C., and Kemp, C.: Undercutting of marine-terminating glaciers in West Greenland, Geophysical Research Letters, 42, 5909–5917, doi:10.1002/2015GL064236, 2015b.

Schoof, C.: Ice-sheet acceleration driven by melt supply variability, Nature, 468, 803–806, doi:10.1038/nature09618, http://www.nature.com/doifinder/10.1038/nature09618, 2010.

Sciascia, R., Straneo, F., Cenedese, C., and Heimbach, P.: Seasonal variability of submarine melt rate and circulation in an East Greenland fjord, Journal of Geophysical Research: Oceans, 118, 2492–2506, doi:10.1002/jgrc.20142, http://doi.wiley.com/10.1002/jgrc.20142, 2013a.

Sciascia, R., Straneo, F., Cenedese, C., and Heimbach, P.: Seasonal variability of submarine melt rate and circulation in an East Greenland fjord, Journal of Geophysical Research: Oceans, 118, 2492–2506, doi:10.1002/jgrc.20142, http://doi.wiley.com/10.1002/jgrc.20142, 2013b.

Slater, D. A., Nienow, P. W., Cowton, T. R., Goldberg, D. N., and Sole, A. J.: Effect of near-terminus subglacial hydrology on tidewater glacier submarine melt rates, Geophysical Research Letters, 42, 2861–2868, doi:10.1002/2014GL062494, 2015.

Slater, D. A., Goldberg, D. N., Nienow, P. W., and Cowton, T. R.: Scalings for Submarine Melting at Tidewater Glaciers from Buoyant Plume Theory, pp. 1839–1855, doi:10.1175/JPO-D-15-0132.1, 2016.

Sole, A. J., Mair, D. W. F., Nienow, P. W., Bartholomew, I. D., King, M. A., Burke, M. J., and Joughin, I.: Seasonal speedup of a Greenland marine-terminating outlet glacier forced by surface melt-induced changes in subglacial hydrology, Journal of Geophysical Research: Earth Surface, 116, 1–11, doi:10.1029/2010JF001948, 2011.

Stevens, L. A., Straneo, F., Das, S. B., Plueddemann, A. J., and Kukulya, A. L.: Linking glacially modified waters to catchment-scale subglacial discharge using autonomous underwater vehicle observations, The Cryosphere, 10, 417–432, doi:10.5194/tc-10-417-2016, http://www.the-cryosphere.net/10/417/2016/, 2016.

Straneo, F. and Heimbach, P.: North Atlantic warming and the retreat of Greenland's outlet glaciers., Nature, 504, 36–43, doi:10.1038/nature12854, http://www.ncbi.nlm.nih.gov/pubmed/24305146, 2013.

Straneo, F., Sutherland, D. a., Holland, D., Gladish, C., Hamilton, G. S., Johnson, H. L., Rignot, E., Xu, Y., and Koppes, M.: Characteristics of ocean waters reaching greenland's glaciers, Annals of Glaciology, 53, 202–210, doi:10.3189/2012AoG60A059, 2012.

Sutherland, D. a. and Straneo, F.: Estimating ocean heat transports and submarine melt rates in sermilik fjord, greenland, using lowered acoustic doppler current profiler (LADCP) velocity profiles, Annals of Glaciology, 53, 50–58, doi:10.3189/2012AoG60A050, 2012.

Turner, J.: Buoyancy effects in fluids, Cambridge University Press, 1973.

Xu, Y., Rignot, E., Menemenlis, D., and Koppes, M.: Numerical experiments on subaqueous melting of Greenland tidewater glaciers in response to ocean warming and enhanced subglacial discharge, Annals of Glaciology, 53, 229–234, doi:10.3189/2012AoG60A139, http://openurl.ingenta.com/content/xref?genre=article{&}issn=0260-3055{&}volume=53{&}issue=60{&}spage=229, 2012.

Xu, Y., Rignot, E., Fenty, I., Menemenlis, D., and Flexas, M. M.: Subaqueous melting of Store Glacier, west Greenland from three-dimensional, high-resolution numerical modeling and ocean observations, Geophysical Research Letters, 40, 4648–4653, doi:10.1002/grl.50825, http://doi.wiley.com/10.1002/grl.50825, 2013.

~~Conceptual scheme of 1D plume model after ?.Uniformly distributed along the grounding line subglacial freshwater flux q_{sg}, enters the fjord and forms a plume that rises up due to buoyancy. The plume is described explicitly with its temperature T, salinity S, thickness D and velocity U. The plume rises along the ice shelf an slope $\alpha = 90° - \beta$ until it either reaches the water surface or has zero velocity due to the loss its buoyancy. The ambient water with salinity S_a and temperature T_a entrains into the plume with an entrainment rate $\dot{e}$. Melting $\dot{m}$ occurs on the glacier front and adds to the plume buoyancy with water of the temperature T_b and salinity S_b.~~

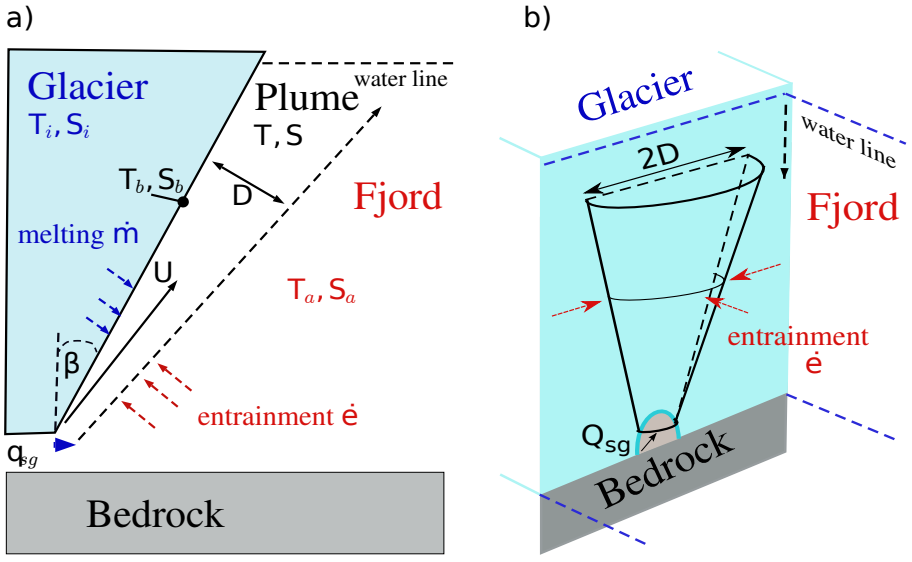

Figure 1. a) Conceptual scheme of 1D plume model after Jenkins (2011).Uniformly distributed along the grounding line subglacial freshwater flux q_{sg}, enters the fjord and forms a plume that rises up due to buoyancy. The plume is described explicitly with its temperature T, salinity S, thickness D and velocity U. The plume rises along the ice shelf an slope $\alpha = 90° - \beta$ until it either reaches the water surface or has zero velocity due to the loss its buoyancy. The ambient water with salinity S_a and temperature T_a entrains into the plume with an entrainment rate $\dot{e}$. Melting $\dot{m}$ occurs on the glacier front and adds to the plume buoyancy with water of the temperature T_b and salinity S_b. b) Conceptual scheme of two-dimensional CP model modified after Jenkins (1991) and Cowton et al. (2015). Subglacial discharge enters the fjord localized, via a channel. The plume geometry is described as a half cone and and the entrainment occurs around the arc. The subglacial discharge is $Q_{sg} = \frac{D_0^2 U_0 \pi}{2}$ where D_0 is the initial radius and U_0 is the initial velocity~~.~~

~~Cumulative melt rate of the LP model (a) and CP model (b) for $E_0 = 0.1$ with different discharge values for a well-mixed environment with $T_a = 4°C$ and $S_a = 34.65$ psu. For the LP (a) red line corresponds $\dot{m} = 6.6 \cdot 10^{-5} \cdot Q_{sg}^{\frac{1}{3}} + 6.0 \cdot 10^{-6}$. For the CP (b) the red line corresponds to $\dot{m} = 0.19 \cdot Q_{sg}^{\frac{2}{5}} + 0.09$. The inset presents the melt rate for small discharges on logarithmic scale. The grey dashed line (a) is our analytical solution for the cumulative melt rate of the LP model (Eq. A20)~~

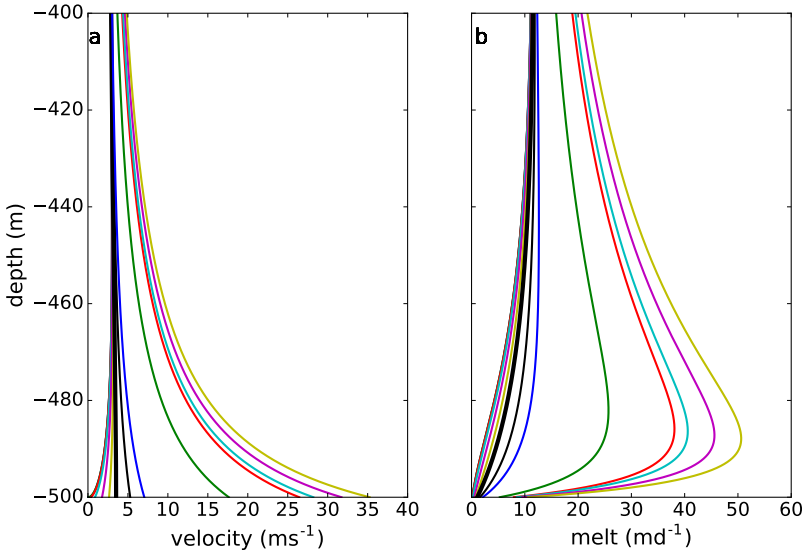

Figure 2. Different runs of the CP model for different initial velocities. Panel a) depicts the velocity profile in the first 100 m. All starting velocities converge within 100 m to the trajectory of the balance velocity ~~$U_b = 3.5\,\mathrm{ms}^{-1}$~~ $U_{*0} = 3.5\,\mathrm{ms}^{-1}$ (thick black ~~, vertical~~ line). The corresponding initial radii differ thus from 300 m (for $U_0 = 3.5\,\mathrm{ms}^{-3}$) to 3 m (for $U_0 = 35\,\mathrm{ms}^{-1}$). Panel b) shows the corresponding melt profile. Higher initial velocities give a maximal melt rates at deeper levels. All melt rate profiles converge to the same melt rate after a certain depth.

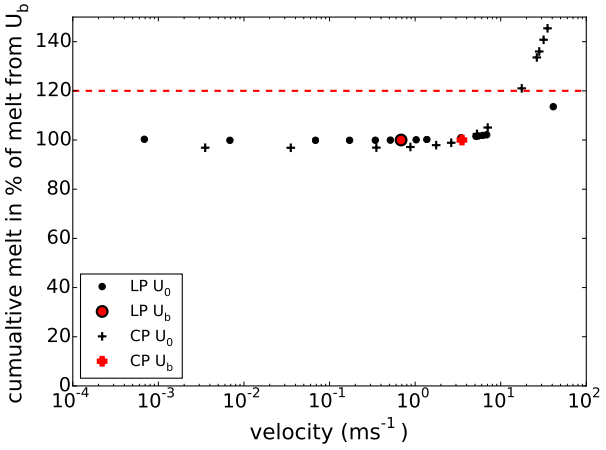

Figure 3. Sensitivity of cumulative melt rate to different initial velocities, for both plume models. Melt rate (black) is in percent of the cumulative melt achieved with initial balance velocity ~~U_b~~ U_* (red). Red dashed line shows 120 % mark. Only very high initial velocities can for the CP model appreciably increase the cumulative melt rate.

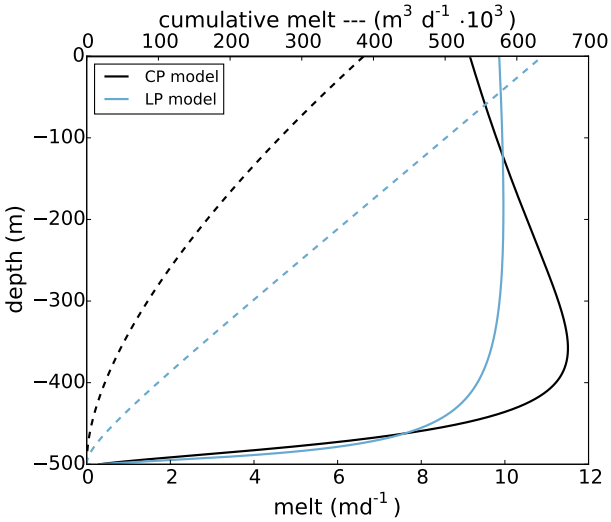

Figure 4. Melt rate profiles in a well-mixed fjord simulated by the CP model (black) and LP model (blue) for a width $W = 150\,\mathrm{m}$ and the total discharge of $Q_{sg} = 500\,\mathrm{m^3 s^{-1}}$. In the case of the CP model the total discharge occur through one channel in the center of the glacier, in the case of LP model the discharge is uniformly distributed with the rate $q_{sg} = \frac{Q_{sg}}{W} = 3.6\,\mathrm{m^2 s^{-1}}$. Both plumes start with a velocity of $U_0 = 1\frac{m}{s}$.Solid lines show melt rate averaged acrosss the plume in the case of CP model and over entire glacier in the case of LP model. The dashed lines shows the corresponding cumulative melt rate for the entire glacier.

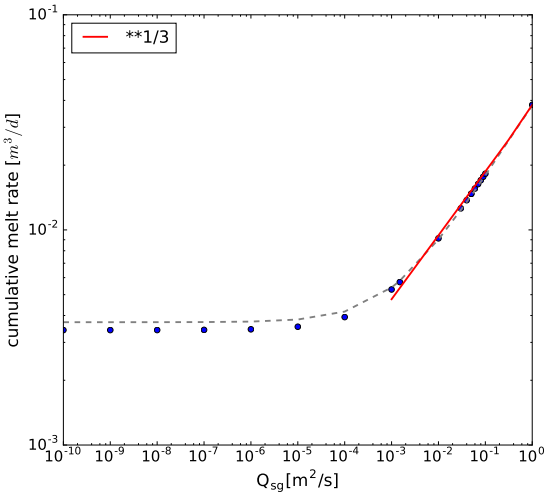

Figure 5. Cumulative melt rate of the LP model (a) for $E_0 = 0.1$ with different discharge values for a well-mixed environment with $T_a = 4°\mathrm{C}$ and $S_a = 34.65$ psu. For red line corresponds $\dot{m} = 6.6 \cdot 10^{-5} \cdot Q_{sg}^{\frac{1}{3}} + 6.0 \cdot 10^{-6}$ for the higher discharge range. The grey dashed line (a) is our analytical solution for the cumulative melt rate of the LP model (Eq. A20)

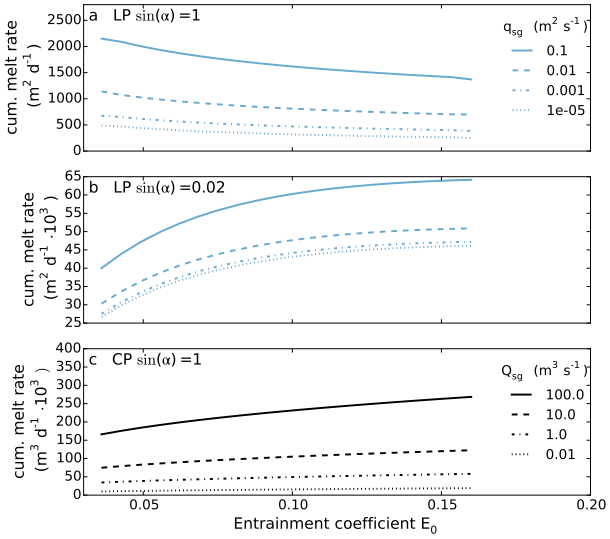

Figure 6. Cumulative melt rates of the different plume models as a function of the entrainment rate factor E_0 for four different discharge values. The cumulative melt rate is depicted for a) LP of a tidewater glacier ($sin(\alpha) = 1$), b) LP of a long floating tongue and c) CP of a tidewater glacier. For the LP model for $sin(\alpha) = 1$ a higher E_0 leads to lower cumulative melting opposite to the other two cases.

~~a) melt rate profile of a plume and its b) velocity, c) thickness and d) temperature computed with the LP model with a discharge $q_{sg} = 10^{-3}\,\mathrm{m}^2\mathrm{s}^{-1}$ for different E_0. Higher E_0 leads to lower melting and slower velocity (b) but thicker (c) and warmer (d) plumes.~~

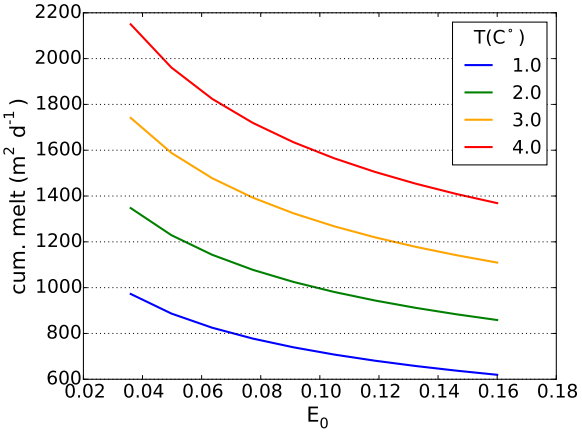

Figure 7. cumulative melt rate in dependence of the entrainment E_0 for $q_{sg} = 10^{-3}\mathrm{m}^2\mathrm{s}^{-1}$ in four different well mixed ambient Temperatures (T_a)

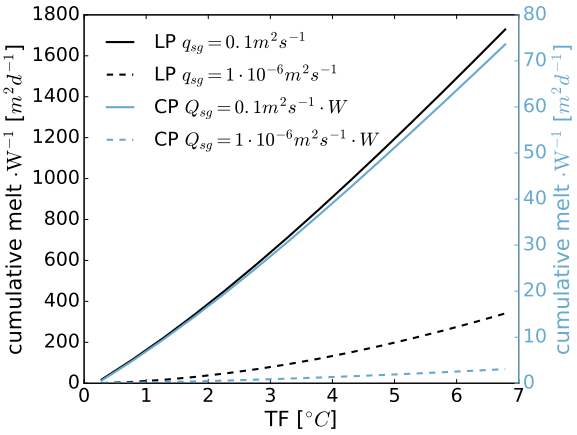

Figure 8. Cumulative melt rate per glacier width W for the LP model (black) and CP (blue) model as a function of the ~~ambient temperature T_a~~ thermal forcing ($TF = T_a - T_{af}$) for high (solid lines) and low (dashed lines) discharge values. The experiment is for a well-mixed, 500m deep and 5km wide tidewater glacier ($\sin(\alpha) = 1$), with $S_a = 34$ psu and $E_0 = 0.1$.

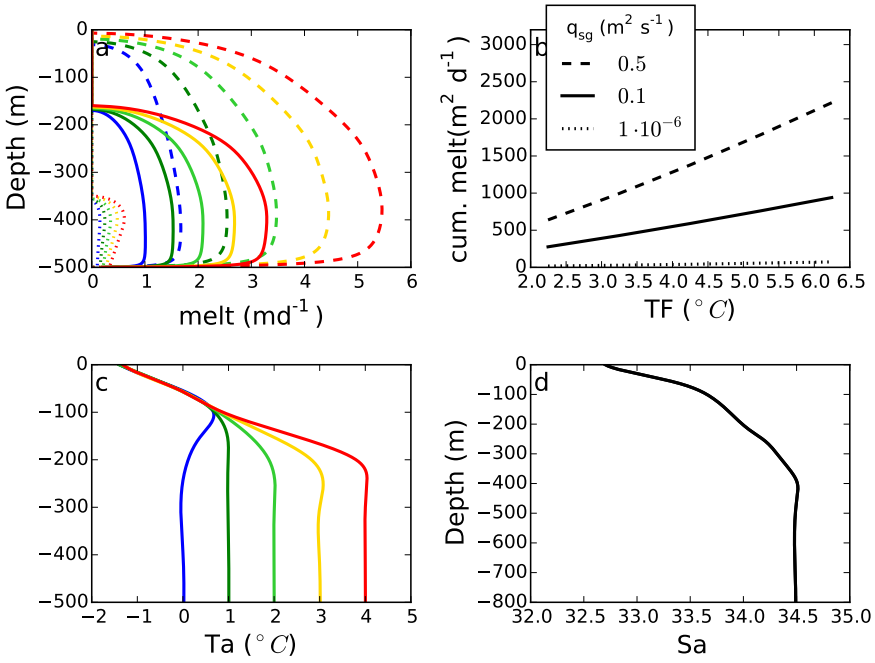

Figure 9. Influence of stratification and discharge on the melt rate profile of the LP (a) . The three different discharge values ($q_{sg} = 0.5, 0.1, 10^{-6}\,\mathrm{m^2 s^{-1}}$, dashed, solid, dotted) in a stratified environment for a fixed salinity profile (d) and 5 different temperature profiles (c) result in 15 different melt rate profiles. The melt rate of the corresponding temperature profile is displayed in the same color as well as in the same style (dashed,dotted or solid) for the corresponding discharge. Note that a very high discharge ($q_{sg} = 0.5\,\mathrm{m^2 s^{-1}}$) is needed for the plume to reach the surface. For each discharge value the corresponding cumulative melt rate is depicted (b) as a function of the thermal forcing ($TF = T_a - T_b$, eq. 7) at the grounding line. For $\dot{m} \sim TF^{\beta}$ we found β values of 1.2 for ($q_{sg} = 0.5\,\mathrm{m^2 s^{-1}}$), 1.2 for ($q_{sg} = 0.1\,\mathrm{m^2 s^{-1}}$) and 1.4 for ($q_{sg} = 10^{-6}\,\mathrm{m^2 s^{-1}}$).

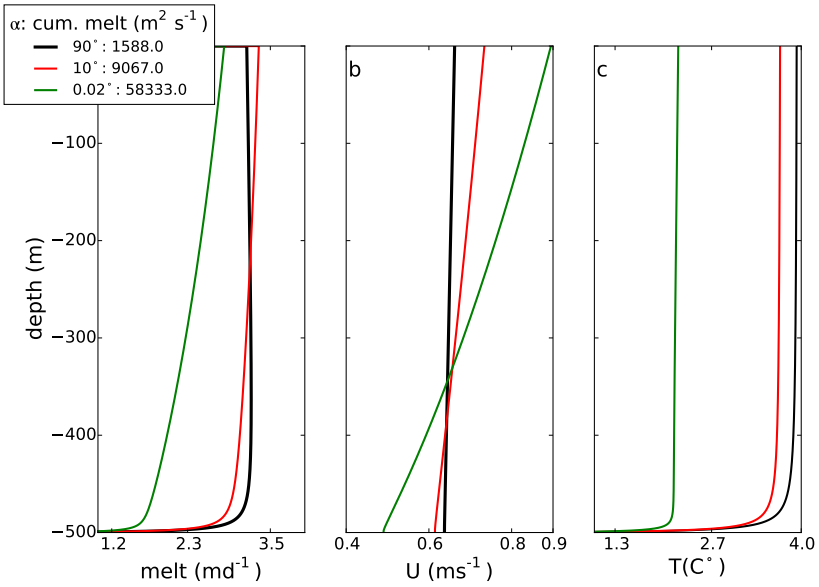

Figure 10. Melt profile (a) and corresponding plume velocity profiles (b) plume temperature (c) and salinity (d) for the LP model for different glacier types: a tide water glacier ($\alpha = 90°$), shelf glacier $\alpha = 10°$ and a shelf glacier with a long floating tongue ($\alpha = 1.1°$) of 25 km. The fjord is well mixed with $Ta = 4°\mathrm{C}$, $Sa = 34.2\,\mathrm{psu}$ and the discharge was set to $q_{sg} = 0.1\,\mathrm{m^2 s^{-1}}$ with $E_0 = 0.1$. Note that the profiles of $\alpha = 90°$ and $\alpha = 10°$ are very similar but the cumulative melt rate of the shelf glacier increased by 500 %. For the long floating tongue the cumulative melt rate is an order of magnitude higher. The grey dashed lines indicate $T_\star$ and $S_\star$ (A2.1.)

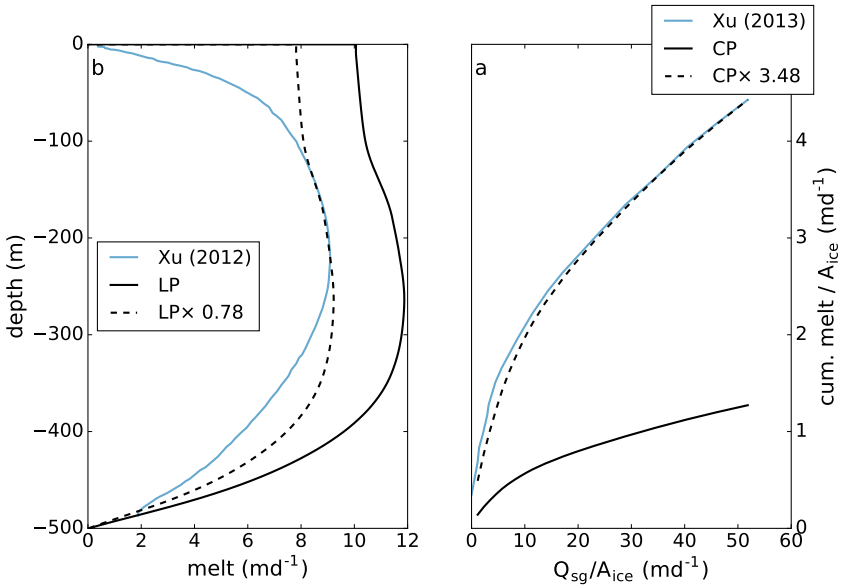

Figure 11. Comparison between LP,CP and GCM simulations. a) ~~Melt profile from Sciascia et al. (2013a) (blue) in comparision with the LP model results (black,solid) for the same temperature and salinity profiles and $q_{sg} = 0.43\,\mathrm{m^2 s^{-1}}$, $E_0 = 0.07$. A scaling factor of 0.47 for the LP model (black, dashed line) is needed to reproduce the results of Sciascia et al. (2013a).~~ b) Experimental results from Xu et al. (2012) (blue line) and LP model (black, solid line) for ($Q_{sg} = \frac{150}{5} = 30\,\mathrm{m^2 s^{-1}}$) and $E0 = 0.07$, $U_0 = 3\,\mathrm{ms^{-1}}$ and the same temperature profile as in Xu et al. (2012). A scaling factor of 0.74 is needed to match the two melt profiles (black, dashed line).b) Average melt rate over a 150 m wide and 500 m deep glacier part as a funciton of discharge localized in one channel. Following Xu et al. (2013), for the x-axis, the discharge Q_{sg} was divided by the area of the ice face $A_{ice} = 150 * 500\,\mathrm{m^2}$ so that $q_{sg} = 50\,\mathrm{md^{-1}}$ corresponds $Q_{sg} = 43.4\,\mathrm{m^3 s^{-1}}$. The numerical results of Xu et al. (2013) are displayed with the blue line. Taking the same conditions (T_a, S_a, Q_{sg}) and an entrainment factor of $E_0 = 0.1$ the CP model gives the solid black line. To match the experiment a scaling factor of 3.40 is needed (black, dashed line).

~~Average melt rate over a 150 m wide and 500 m deep glacier part as a funciton of discharge localized in one channel. Following Xu et al. (2013), for the x-axis, the discharge Q_{sg} was divided by the area of the ice face $A_{ice} = 150 * 500\,\mathrm{m}^2$ so that $q_{sq} = 50\,\mathrm{md}^{-1}$ corresponds $Q_{sg} = 43.4\,\mathrm{m}^3\mathrm{s}^{-1}$. The numerical results of Xu et al. (2013) are displayed with the blue line. Taking the same conditions (T_a, S_a, Q_{sg}) and an entrainment factor of $E_0 = 0.1$ the CP model gives the solid black line. To match the experiment a scaling factor of 3.40 is needed (black, dashed line).~~

~~Average melt rate over a 2km wide and 500m deep glacier (A_{ice}) as a function of the channel number with a total discharge of $Q_{sg} = 500\,\mathrm{m}^3\mathrm{s}^{-1}$.The numerical experiment from Slater et al. (2015) (blue) and CP model (black).Taking the same conditions (T_a, S_a, Q_{sg}) and an entrainment factor of $E_0 = 0.1$ the CP model was run (black, solid line). Note that for a an increasing number of channels n the discharge as input to the CP model is $Q_{sg} = 500\,\mathrm{m}^3\mathrm{s}^{-1}$ divided by n the number of channels and the total melt is multiplied by n. To match the resulat of Slater et al. (2015) in the lower range of channel numbers a scaling factor of 2.48 is needed (black, dashed line). The total discharge distributed over the whole glacier width $q_{sq} = \frac{500}{2000} = 0.25\,\mathrm{m}^2\mathrm{s}^{-1}$ gives a melt rate for the LP model (red, dahed line) that still underestimates the corresponding melt rate in Slater et al. (2015) (value of blue line crossing the y-axis).~~

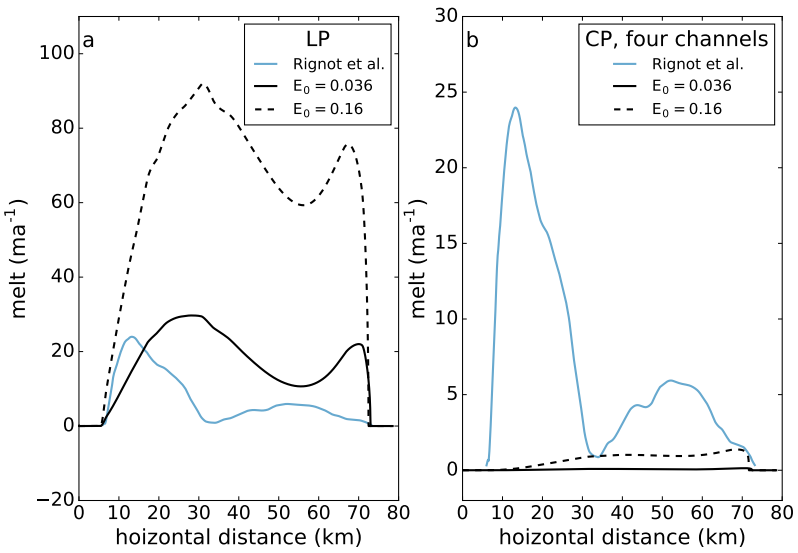

Figure 12. Melt rate of a) LP model simulated over the long floating tongue of Petermann glacier with a minimal discharge of $Q_{min} = 10^{-5}\,\mathrm{m}^2\mathrm{s}^{-1}$ for the minimal ($E_0 = 0.036$) and maximal ($E_0 = 0.16$) value (black lines) of the entrainement parameter. In panel b) we used the maximum discharge $Q_{sg} = 296\,\mathrm{m}^3\mathrm{s}^{-1}$ (total runoff assumed only in summer) distributed over four channels to compute the melt rate with the CP model. As forcing variables we used the fjord's temperature and salinity profile in front of the floating tongue for the year 2003 summarized by Johnson et al. (2011a) and from Morlighem et al. (2014) we determined the glacier thickness and depth of the floating tongue (see 5.1 for details). For both E_0 the melt rate is highly overestimated with the LP model and underestimated with the CP model. The empirical melt rate estimated by Rignot and Steffen (2008) is displayed with the blue line. Note the different vertical scale on the panels.

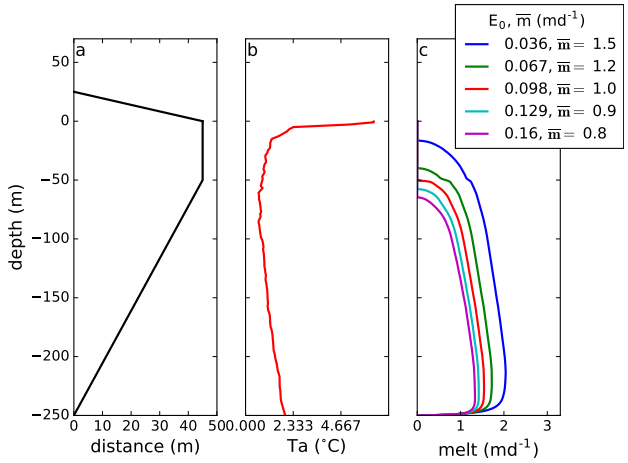

Figure 13. Kangerlussuup Sermia average undercut profile at the terminus (a) with the assumed temperature profile (b) give different melt rate profiles (c) simulated for different E_0 and same $Q_{sg} = 208\,\mathrm{m^3 s^{-1}}$. All average melt rates are below the determined $2\,\mathrm{md^{-1}}$ by Fried et al. (2015).

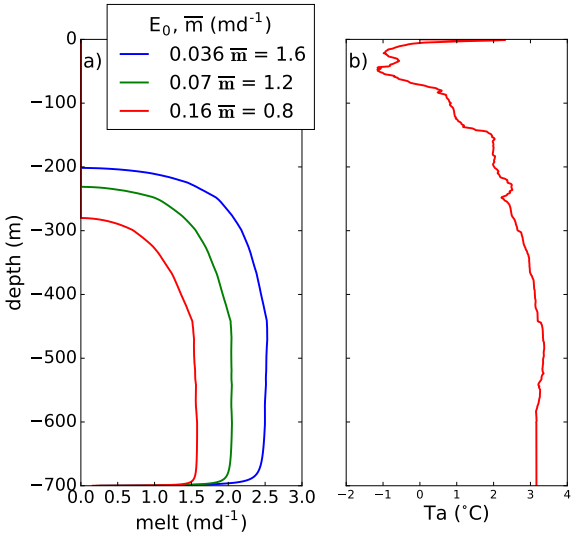

Figure 14. Three vertical melt rate profiles of the LP model (a) for three different entrainment coefficients E_0 for Helheim glacier. With and discharge of $2.69 \cdot 10^{-2} m^2 s^{-1}$ ~~$E_0 = 0.04$~~ and $E_0 = 0.036$ we obtain an average melt rate of ~~$\overline{m} = 1.7\mathrm{ma}^{-1}$~~ ~~equal~~ $\overline{m} = 1.6\mathrm{ma}^{-1}$ very close to Sutherland et. al ($1.7\,\mathrm{md}^{-1}$).

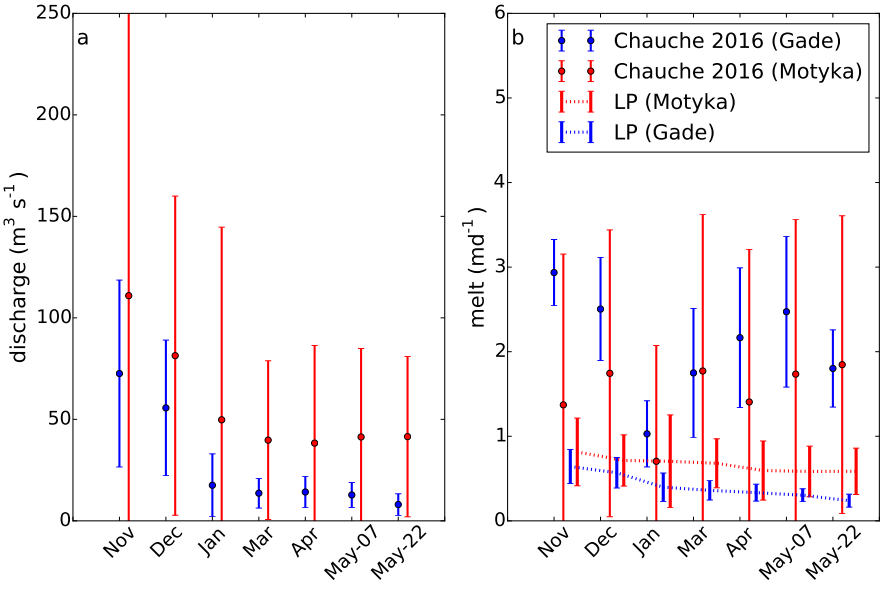

Figure 15. a)Estimated ~~sublgacial~~ subglacial discharge of Store Glacier for winter 2012/2013 in from (Chauche, 2016). Red ranges give sublgacial discharge estimates by the Motyka model and blue ranges by the Gade model and b) the corresponding melt rate profiles. Simulated melt rates by the LP model with E_0=0.036 are depicted in the red dotted (subglacial discharge from Moytka model) and blue dotted (subglacial discharge from Gade model.)

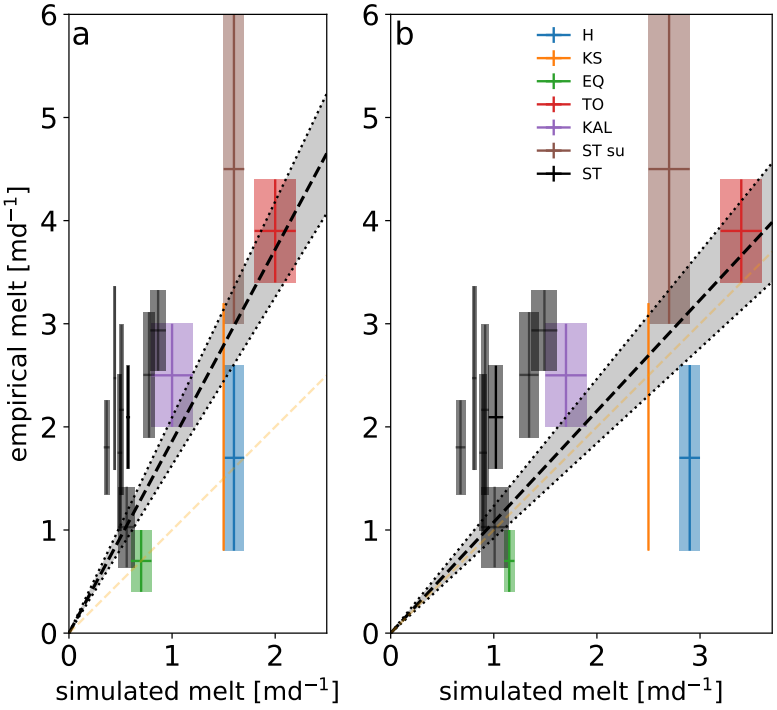

Figure 16. Measured versus simulated melt rate for a number of glaciers, for data given in Table 6. The squares represent error bars in measured and simulated melt rate. The black regression line with 1-sigma uncertainty range indicates the average scaling coefficient required to match observations given model parameters. In both panels, entrainment rate is 0.036. Panel (a) shows model simulations with default values for the heat transfer coefficient $\Gamma_T = 2.2 \cdot 10^{-2}$, while Panel (b) shows simulation with $\Gamma_T = 4.2 \cdot 10^{-2}$, which produces a scaling coefficient closer to one. Glacier abbreviations are shown in Table 6.

Table 1. Model parameters of the LP and CP model with typical fjord default values.

Symbol	Value	Units	Desciption
q_{sg}	0.1	$\frac{m^2}{s}$	default value for subglacial discharge for LP
Q_{sg}	500	$\frac{m^3}{s}$	default value for subglacial discharge for CP
$U_{\star 0}$	–	$\frac{m}{s}$	initial default value for plume velocity
$T\|_{x0}$	0	$^\circ C$	inital default value for plume temperature
T_a	4	$^\circ C$	default value for ambient temperature
$S\|_{x0}$	$1e-6$	psu	default value for ambient salinity
S_a	34.65	psu	default value for ambient salinity
E_0	$0.1[0.036-0.16]$	–	Entrainment coefficient
C_d	$2.5 \cdot 10^{-3}$	–	Drag coefficient
λ_1	$-5.73 \cdot 10^{-2}$	$^\circ C$	Seawater freezing point slope
λ_2	$8.32 \cdot 10^{-2}$	$^\circ C$	Seawater freezing point offset
λ_3	$7.61 \cdot 10^{-4}$	$^\circ C\, m^{-1}$	Depth dependence of freezing point
L	$3.35 \cdot 10^5$	$J\, kg^-1$	Latent heat of fusion for ice
c_i	$2.009 \cdot 10^3$	$J\, kg^{-1}\, K^{-1}$	Specific heat capacity for ice
c	$3.974 \cdot 10^3$	$J\, kg^{-1}\, K^{-1}$	Specific heat capacity for seawater
β_S	$7.86 \cdot 10^{-4}$	–	Haline contraction coefficient
β_T	$3.87 \cdot 10^{-5}$	–	Thermal expansion coefficient
g	9.81	$m\, s^{-2}$	Gravity constant
Γ_T	$2.2 \cdot 10^{-2}$	–	Thermal turbulent transfer coefficient
Γ_S	$6.2 \cdot 10^{-4}$	–	Salt turbulent transfer coefficient

Table 2. Determination of the power law β of melt rate on discharge Q or the equation $\dot{m} = a(b \cdot Q^\beta + c)$.Seperation between high $(Q > Q_c)$ and low discharge $(Q < Q_c)$

$\beta(Q > Q_c)$	$\beta(Q < Q_c)$	Q_c [discharge range]	Experiment
0.54	0.80	~~4.34~~ 5.76 [1-45] $\frac{m^3}{s}$	(Xu et al., 2013)
0.45	0.70	4.34 [1-45] $\frac{m^3}{s}$	CP model
0.33	0.54	$5 \cdot 10^{-5}$ [10^{-5}-1] $\frac{m^2}{s}$	LP model

Table 3. Determination of the power law β of melt rate on thermal forcing $TF = T_a - T_{af}$ or the relation $\bar{m} \propto TF^{\beta}$ for low and high discharge with comparision to theoretical estimated values. Upper eight rows are from this study lower show results of other 3d simulaitons.

discharge	β experimental	β theoretical	Experiment type
high ($q = 0.1 \frac{m^2}{s}$)	1.2[a]	1 [b,c,d]	LP, well mixed
low ($q = 1 \cdot 10^{-6} \frac{m^2}{s}$)	1.8 [a]	1.5[c,d]	LP, well mixed
high ($q = 0.1 \frac{m^2}{s}$)	1.2[a]	2 (linear stratified)[c]	LP, realistic stratified
low ($q = 1 \cdot 10^{-6} \frac{m^2}{s}$)	1.4[a]	2(linear stratified)[c]	LP, realistic stratified
high ($q = 500 \frac{m^3}{s}$)	1.2[a]	1[e]	CP, well mixed
low ($q = 5 \cdot 10^{-3} \frac{m^2}{s}$)	1.5[a]	1[e]	CP, well mixed
high ($q = 500 \frac{m^3}{s}$)	1.1[a]	-	CP, realistic stratified
low ($q = 5 \cdot 10^{-3} \frac{m^2}{s}$)	1.3[a]	-	CP, realistic stratified
high ($q > 5.8 \frac{m^3}{s}$)	1.2[f]	-	3D CP, realistic stratified
low ($q < 5.8 \frac{m^2}{s}$)	1.6[f]	-	3D CP, realistic stratified

[a] this study [b] Jenkins (2011) [c] Magorrian and Wells (2016) [d] chapter A3
[e] Slater et al. (2016) [f] Xu et al. (2013)

Table 4. Simulated cumulative melt rate (%) of empirical estimated cumulative melt rate for different entrainment rates for three West Greenland glaciers.

TOR			KANGIL			EQIP		
model	E_0	melt ratio (%)	model	E_0	melt ratio (%)	model	E_0	melt ratio (%)
LP	0.036	57	LP	0.036	45	LP	0.036	103
CP	0.036	1	CP	0.036	2	CP	0.036	5
LP	0.16	22	LP	0.16	19	LP	0.16	44
CP	0.16	2	CP	0.16	3	CP	0.16	8

Table 5. Comparision of the melt rate calculated with the LP model and the empirical data obtained with the Gade and Motyka model (Chauche, 2016).

	melt (md^{-1}) (Chauche, 2016)	melt (md^{-1}) LP ($E_0 = 0.036$)
Gade	2.2 ± 0.5	~~0.4 ± 0.1~~ 0.6 ± 0.1
Motyka	1.6 ± 0.4	~~0.6 ± 0.4~~ 0.7 ± 0.3
Average	1.9 ± 0.5	~~0.5 ± 0.3~~ 0.7 ± 0.2

Table 6. Measured subglacial discharge Q_{emp} and melt rate m_{emp} for a number of glaciers, and corresponding melt rate m_{lp} from LP model simulations.Values of Store winter are taken from the gade model (Fig. 15). For each glacier, local hydrography (temperature and salinity profiles) and measured sublacial discharge is used to drive the LP model. Ranges indicate measurement errors. Errors in subglacial discharge are propagated to errors in simulated melt rate via the LP model. Simulated melt rate m_{LP} is obtained with $E_0 = 0.036$, $\Gamma_\mathcal{T} = 2.2$. Melt rate $m^\star_{LP}$ with modified $\Gamma_\mathcal{T} = 4.2$ is also provided.

	$\mathrm{Q_{emp.}}$ [$\mathrm{m^3/s}$]	$\mathrm{m_{emp.}}$ [m/d]	$\mathrm{m_{LP}}$ [m/d]	$\mathrm{m^\star_{LP}}$ [m/d]
Helheim (H)	137 -189	0.7-2.6	1.6-1.7	XX
Kangerlussuup Sermia (KS)	208	0.8-3.2	1.5	XX
Equip Sermia(EQ)	101-121	0.4-1.0	0.7-0.8	XX
Seermeq Avangnardleq and Sermeq Kujatdleq (TO)	559-679	3.4-4.4	2.0-2.2	XX
Kangilerngata Sermia (KAL)	208-328	1.9-3.0	1.0-1.2	XX
Store (Winter) (ST)	3-250	1.5-2.4	0.5-0.8	XX
Store (Summer) (ST su)	201-291	3.0-6.0	1.4-3.0	XX

Table A1. Summary of appendix variables. Illustrative value provided for $T_i = -15^{\circ}C$, $T_a = 4^{\circ}C$, $S_a = 34.65$ psu, $\sin\alpha = 1$ (tide water glacier), and range for $E_0 = 0.036 - 0.16$

Symbol	Definition	Interpretation	Illustrative Value
M_0	-	melt rate coefficient in (A1)	$8.2 \cdot 10^{-6}\ ^{\circ}C^{-1}$
b_0	$g \sin\alpha(\beta_S S_a - \beta_T T_a)$	buoyancy at $x = 0$	0.27 ms^{-2}
b_m	$g \sin\alpha(\beta_S S_a - \beta_T (T_a - T_m))$	buoyancy source term due to melting	0.23 ms^{-2}
T_m	$c_i/cT_i - L/c$	effective meltwater temperature	$-0.9 \cdot 10^2\ ^{\circ}C$
T_e	$\frac{E_0}{M_0} \sin\alpha$	entrainment-equivalent temperature	$4.4 \cdot 10^3 - 2.0 \cdot 10^4\ ^{\circ}C$
C_e	$E_0 \sin\alpha$	effective entrainment	0.036 - 0.16
ΔT_a	$T_a - T_f(S_a)$	ambient temperature above freezing	$\approx 6\ ^{\circ}C$

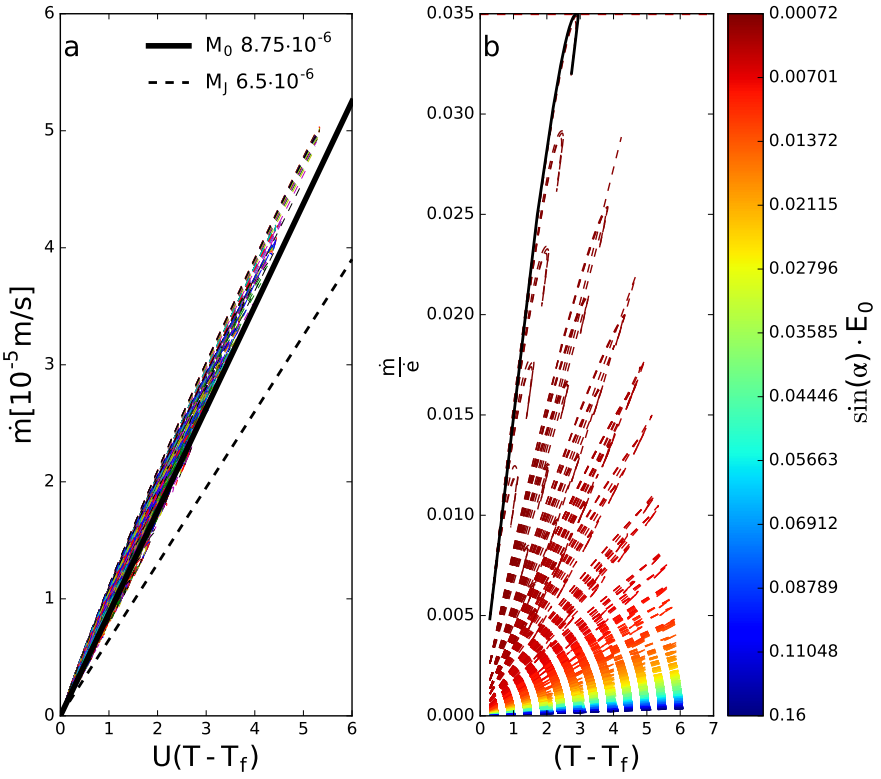

Figure A1. Investigation of melting proportion in the plume equations for different LP experiments. The plume model was run in a well mixed environment for different parameter settings: $E0[0.036 - 0.16]$, $sin(\alpha)[0.02 - 1]$, $q_{sq}[10^{-5} - 0.1\frac{m^2}{s}]$, $T_a[0 - 4]^{\circ}C$. Panel a) shows the melt rate as a function of plume velocity U and plume temperature T and it's freezing temperature T_f ($\dot{m} = M_0(T - T_f)U$). The second panel illustrates that $\dot{m} << \dot{e}$ in this parameter range,but beeing biggest for long floating tongues.

~~Convergence of melt rate (a), velocity (b), temperature (c) and salinity (d) within the first 50 meter of the LP.~~

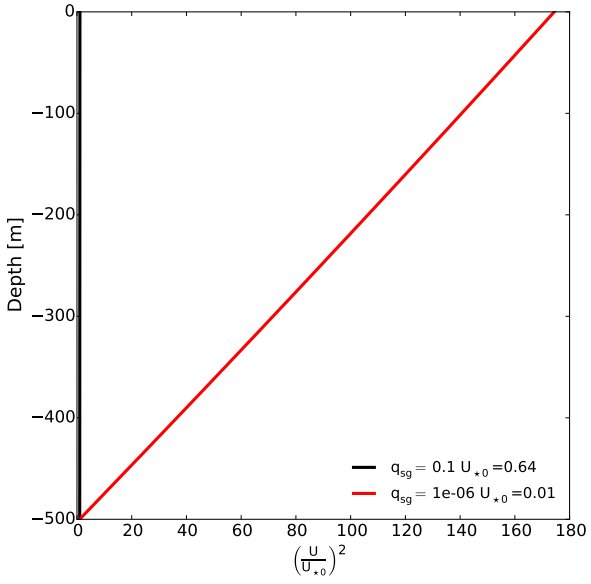

Figure A2. Evolution of U for an initial velocity of $U_\star$. The plume with a small discharge ($q_{sg} = 10^{-6}\,\frac{m^2}{s}$) will accelerate strongly (red line,$U_\star = 0.14\,\frac{m}{s}$) while the plume velocity with larger discharge remains almost constant (black line, $q_{sg} = 0.1\,\frac{m^2}{s}$, ,$U_\star = 0.63\,\frac{m}{s}$).

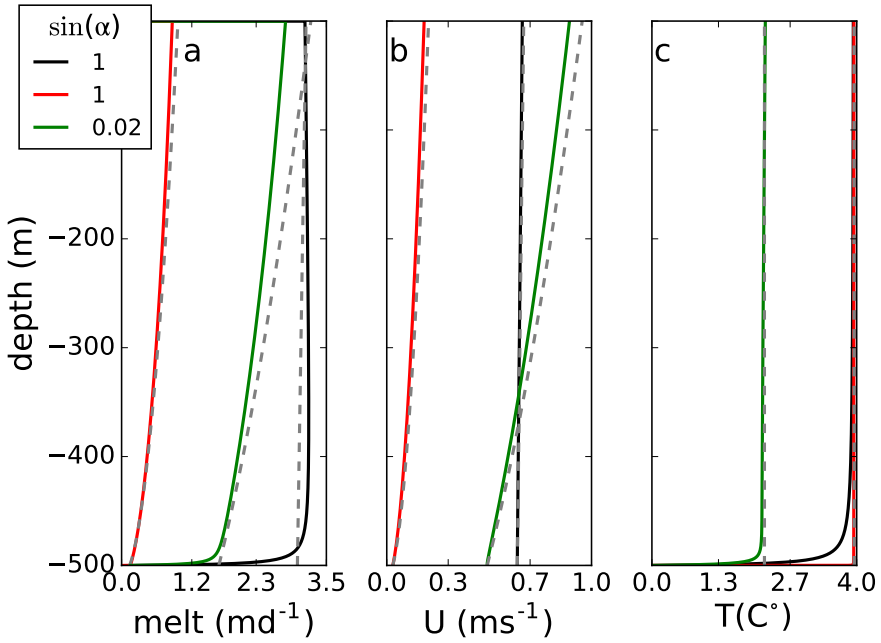

Figure A3. Evolution of m (a), U(b) and T(c) along Z for the tidewater glaciers with high discharge ($q_{sg} = 0.1 \frac{m^2}{s}$, black line), low discharge ($q_{sg} = 10^{-5} \frac{m^2}{s}$,red line) and a floating tongue glacier ($q_{sg} = 0.1 \frac{m^2}{s}$, green line). The corresponding approximations of $m_\star = M_0 U_\star \Delta T_\star$, $U_\star$ (A13), $T_\star$ (A9) (grey, dashed line) show high similarities.